A Search for Genes Mediating the Growth-Promoting Function of TGFβ in the *Drosophila melanogaster* Wing Disc

Covadonga F. Hevia,[1] Ana López-Varea, Nuria Esteban, and Jose F. de Celis[2]
Centro de Biología Molecular Severo Ochoa, Consejo Superior de Investigaciones Científicas and Universidad Autónoma de Madrid, 28049, Spain
ORCID IDs: 0000-0003-4322-2415 (C.F.H.); 0000-0003-4808-9844 (J.F.d.C.)

ABSTRACT Transforming Growth Factor β (TGFβ) signaling has a complex influence on cell proliferation, acting to stop cell division in differentiating cells, but also promoting cell division in immature cells. The activity of the pathway in *Drosophila* is mostly required to stimulate the proliferation of neural and epithelial tissues. Most interestingly, this function is not absolutely required for cell division, but it is needed for these tissues to reach their correct size. It is not known how TGFβ signaling promotes cell division in imaginal discs, or what the interactions between TGFβ activity and other signaling pathways regulating cell proliferation are. In this work, we have explored the disc autonomous function of TGFβ that promotes wing imaginal disc growth. We have studied the genetic interactions between TGFβ signaling and other pathways regulating wing disc growth, such as the Insulin and Hippo/Salvador/Warts pathways, as well as cell cycle regulators. We have also identified a collection of TGFβ candidate target genes affecting imaginal growth using expression profiles. These candidates correspond to genes participating in the regulation of a variety of biochemical processes, including different aspects of cell metabolism, suggesting that TGFβ could affect cell proliferation by regulating the metabolic fitness of imaginal cells.

KEYWORDS TGFβ; Smad2; growth control; microarray analysis; imaginal disc

THE *Drosophila* wing is an excellent organ to identify and analyze the cellular and biochemical bases of tissue size regulation (Edgar 2006; Neto-Silva *et al.* 2009). The wing is the result of the differentiation during metamorphosis of a simple epithelium, the wing imaginal disc, and consequently the size of the wing is determined by the mechanisms controlling the growth of this epithelial tissue (Johnston and Gallant 2002). The wing disc is specified during embryonic development as a group of ectodermal cells, and this primordium proliferates during larval development following a stereotyped pattern of cell divisions (Milan *et al.* 1996). The wing disc is highly plastic to genetic and environmental conditions and its final size is determined by two parameters: cell size, which is related to cellular growth, and cell number, which is determined by cell division (Edgar *et al.* 2001). Both aspects are subject and/or influenced by a variety of regulatory mechanisms, which act exclusively within the epithelium ("intrinsic mechanisms") or that integrate hormonal and environmental cues in the growing epithelium ("extrinsic mechanisms") (Bryant and Simpson 1984; Edgar *et al.* 2001). Genetic analysis has identified many of the relevant players affecting cell growth and cell division, including cell cycle regulators, signaling pathways, hormones, and a limited set of transcription factors (Molnar *et al.* 2011). Not surprisingly, mutations in the corresponding human orthologous genes have major consequences for health; consequently, understanding the precise contribution that each one has on cell growth and division is of major biomedical relevance (Molnar *et al.* 2011).

The activity of signaling pathways impinging on cell division and growth is of particular importance in the control of wing size. Some of these pathways affect the progression of

doi: https://doi.org/10.1534/genetics.116.197228
Manuscript received October 25, 2016; accepted for publication March 9, 2017; published Early Online March 16, 2017.
Supplemental material is available online at www.genetics.org/lookup/suppl/doi:10.1534/genetics.116.197228/-/DC1.
[1]Present address: Department of Experimental and Health Sciences, Universitat Pompeu Fabra, Parc de Recerca Biomèdica de Barcelona, 08003-Barcelona, Spain.
[2]Corresponding author: Centro de Biología Molecular Severo Ochoa, calle Nicolás Cabrera 1, Universidad Autónoma de Madrid, Madrid 28049, Spain. E-mail: jfdecelis@cbm.csic.es

the cell cycle and the growth of the cell in manners that are not entirely clear. This is the case of the EGFR and insulin receptor (InR) signaling pathways, which are the principal regulators of cell size but also have major effects in the control of cell division (Leevers *et al.* 1999; Prober and Edgar 2002; Orme *et al.* 2006). Other pathways mostly regulate cell proliferation without compromising or with minor effects on cellular growth. A paradigmatic example is the Hippo/Salvador/Warts (HSW) pathway, a molecular device that translates, through the activity of the Yorkie transcription coactivator, molecular forces within the epithelium into the regulation of both cell cycle progression and inhibition of apoptosis (Oh and Irvine 2010; Chen *et al.* 2012). Other pathways that have key roles during the patterning of the epithelium also influence cell division. This is the case of the decapentaplegic/bone morphogenetic protein (Dpp/BMP), Notch, Wingless (Wnt), and JAK/STAT (Janus kinase/signal transducer and activator of transcription) signaling pathways, which affect cell proliferation in the entire wing (Dpp and Notch) or mostly in the proximal part of the wing, the hinge (Wnt and JAK/STAT) (Molnar *et al.* 2011). It is not known how the information provided by each one of these pathways is integrated within the cell to regulate its division. This problem is far from being resolved because we still do not know which are the relevant genes regulated by the transcription factors acting as final transducers of these pathways.

One of the pathways that has a major impact on the regulation of cell proliferation during development is the Transforming Growth Factor β (TGFβ)/Activin signaling pathway (Shi and Massagué 2003). The TGFβ pathway has been extensively studied in different organisms and in a multitude of cellular settings, and we have a fairly complete molecular description of its components, biological requirements, and mechanisms of action (Shi and Massagué 2003). The TGFβ pathway in *Drosophila* includes the ligands Activin-β (Actβ; CG11062), Dawdle (daw; CG16987), Maverick (mav; CG1901), and Myoglianin (myo; CG1838); the receptor complex formed by Baboon (babo; CG8224) and Punt (put; CG7904); and the transducers Smad on X (Smad2; CG2262) and Medea (Med; CG1775). Essentially, pathway activation results in the generation of a Smad2/Med transcriptional complex that localizes to the nucleus and can interact with the DNA to regulate gene expression. The apparent simplicity from the genetic point of view hides tremendous complexity in the biology of ligand and receptor interactions and in the molecular mechanisms regulating the transcriptional response to the pathway (Feng and Derynck 2005; Massagué 2012). Thus, although the Smad proteins can bind to DNA, the affinity of Smad complexes/DNA is low, and consequently Smad proteins usually associate with other transcriptional regulators to efficiently interact with the regulatory regions of their target genes. This mode of action, as well as the capacity of Smads to recruit a multitude of corepressors, coactivators, and chromatin remodelling protein complexes, confers an enormous versatility to the biological responses to the pathway, and also implies that these responses are highly dependent on the cellular context in which the pathway operates (Feng and Derynck 2005; Massagué 2012).

The best-characterized role of TGFβ signaling in the regulation of cell division was identified in cell culture experiments, where it negatively regulates cell cycle progression in hematopoietic, neural, and epithelial cells through the transcriptional control of several cyclin-dependent kinase inhibitors (Massagué and Wotton 2000; Derynck *et al.* 2001). In stark contrast, the activity of the pathway in *Drosophila* is mostly required to promote the proliferation of neural and epithelial tissues (Brummel *et al.* 1999; Zhu *et al.* 2008). Intriguingly, in both cases, this activity is not absolutely required for cell division, but it is needed for these tissues to reach their correct size. A similar requirement for mouse and human embryonic stem cell proliferation suggests that TGFβ activity stops cell division in cells primed to differentiate, but promotes cell division in cells with stem cell characteristics. In the particular case of the *Drosophila* wing disc, TGFβ signaling has two independent functions that result in the promotion of cell proliferation. On the one hand, TGFβ signaling is required in the ring gland, the main endocrine organ of the *Drosophila* larva, where it regulates the production of the steroid hormone Ecdyson (Gibbens *et al.* 2011). Ecdyson not only promotes the progression through larval stages and metamorphosis, but is also required in the imaginal discs to sustain cell proliferation in the third larval instar (Herboso *et al.* 2015). On the other hand, TGFβ signaling acting in epithelial cells is also required for the wing disc to reach its normal size (Brummel *et al.* 1999; Hevia and de Celis 2013). In this manner, the ring gland and the wing epithelium are places of ligand production and accumulate phosphorylated Smad2 (Brummel *et al.* 1999; Hevia and de Celis 2013).

In this work, we have explored the autonomous function of TGFβ signaling that promotes imaginal disc growth. We have studied the genetic interactions between TGFβ signaling and other pathways regulating wing disc growth, such as the InR and HSW pathways, as well as cell cycle regulators. We have also studied the expression profile of wing discs in which the level of Smad2 protein is reduced or its activity is increased, with the aim of identifying candidate Smad2 target genes. We find a numerous and heterogeneous group of genes, the expression of which is activated by Smad2. A considerable fraction of these genes are required for wing disc growth, implying that they are good candidates to mediate the promotion of cell proliferation by TGFβ. The candidates identified as potential mediators of Smad2 activity participate in a variety of biochemical processes linked to cellular physiology and metabolism. In this manner, TGFβ function in the wing coordinates the expression of genes that impinge on the fitness of the epidermal cells, allowing them to sustain their proper proliferation rhythm.

Materials and Methods

Genetic strains and genetic analysis

We used the *Gal4* lines *sal^{EPv}-Gal4*, *nub-Gal4*, *en-Gal4*, *hh-Gal4*, *ap-Gal4*, *dll-Gal4*, and *AB1-Gal4*. The expression of *sal^{EPv}-Gal4* is restricted to the wing blade territory located between the vein L2 and the intervein L4/L5 (Cruz *et al.* 2009), the expression of *nub-Gal4* occurs in the wing pouch and hinge, the expression of *en-Gal4* and *hh-Gal4* is restricted to the posterior compartment of all imaginal discs, the expression of *ap-Gal4* to the dorsal compartment of the wing disc, the expression of *dll-Gal4* localizes to the presumptive tarsi and tibia of the leg imaginal discs (Calleja *et al.* 1996), and the expression of *AB1-Gal4* is limited to the salivary glands. We used the *UAS* lines *UAS-GFP*, *UAS-dicer2*, *UAS-CycE*, *UAS-stg*, *UAS-InR^{DN}* [8252, DBSC (Bloomington *Drosophila* Stock Center)], and *UAS-Smad2^{PM}* (*UAS-dSmad2^{SDVD}*; Gesualdi and Haerry 2007). We also use the following *UAS* lines to express RNA interference for the genes *string* [*UAS-stg-i*; 1395-R2 NIG-FLY (National Institute of Genetics, Japan)], *Smad2* (*UAS-Smad2-i*; 2262R-1, NIG-FLY), *Cyclin E* (*UAS-CycE-i*; 29314, BDSC), *yorkie* [*UAS-yki-i*; 40497-GD, VDRC (Vienna *Drosophila* RNAi Center)], *expanded* (*UAS-ex-i*; 109281-KK, VDRC), *hippo* (*UAS-hpo-i*; 104169-KK, VDRC), and *Pten* (*UAS-Pten-i*; 35731-GD, VDRC). Other UAS-RNAi (RNA interference) lines used are listed in Supplemental Material, Table S1. We also used the reporter lines *diap1-lacZ* (Ryoo *et al.* 2002), *expanded-lacZ* (*ex-lacZ*) (Boedigheimer *et al.* 1993), and *proliferating cell nuclear antigen* (PCNA-GFP) (Thacker *et al.* 2003), and the *Smad2* allele *Smad2^{F4}* (Peterson *et al.* 2012). Janelia Gal4 lines were obtained from BDSC. Lines not described in the text can be found in FlyBase. The loss-of-function phenotypes were determined in *UAS-dicer2/+*; *nub-Gal4/UAS-RNAi* and *UAS-dicer2/+*; *sal^{EPv}-Gal4/UAS-RNAi* combinations. Unless otherwise stated, crosses were done at 25°.

Generation of UAS-HA-Smad2^{PM}

We generated a constitutively activated (phospho-mimic) N-terminally HA-tagged version of Smad2 (*UAS-HA-Smad2^{PM}*) substituting the last two Ser residues (TCC and TCA) of Smad2 to Asp (GAC) by Quick Change Site-Directed Mutagenesis (Stratagene, La Jolla, CA) using the primers 5′-GGCTGCCGTGCAGCGACATGGACTAAGCGCACGGCCG-3′ and 5′-CGGCCGTGCGCTTAGTCCATGTCGCTGCACGGCAGCC-3′; and subsequent cloning in Gateway pTHW vector (Invitrogen, Carlsbad, CA).

Generation of ana-RR-GFP line

The genomic regulatory region chr2R: 4951166-4953561 (*R5/dm3*) was amplified by PCR using the primers 5′-CACCAAAATTTGCATTAAATTAC-3′ and 5′-TCGATTATATGCATCAGTCTGTT-3′, and subsequently cloned in pENTR/D-TOPO vector (Invitrogen). To generate the GFP reporter line, we used the LR Clonase II enzyme to introduce the genomic regulatory region in the pHPdesteGFP vector (Addgene).

Clonal analyses

Clones were generated by flipase (FLP)-induced mitotic recombination in larvae of the following genotypes:

Smad2^{F4} FRT19A/FRT19 AM(1)o^{sp}; nub-Gal4/+; UAS-FLP/+
Smad2F4 FRT19A/FRT19 am(1)osp; dll-Gal4 UAS-FLP/+
Smad2F4 FRT19A/FRT19A Ubi-GFP hs-FLP1.22.

Immunocytochemistry

We used rabbit anti-βGal (1:2000; MP Biomedicals), mouse anti-HA (1:100; Hybridoma bank) and anti-Wg (1:50; Hybridoma bank), ToPro100 to label the nuclei (1:200; Invitrogen), and *phalloidin-TRITC* (1:100) to label F-actin (Sigma [Sigma Chemical], St. Louis, MO). Secondary antibodies were from Jackson Immunological Laboratories (used at 1/200 dilution). Imaginal wing discs were dissected, fixed, and stained as described in de Celis (1997). Confocal images were captured using a LSM510 confocal microscope. All images were processed with the ImageJ 1.46n software (NIH) and Adobe Photoshop CS6.

Wing and disc measurements

Wing size and cell size in adult wings were measured in pixels using the "Analyze" tool in Adobe Photoshop. We analyzed 10 wings from females of each genotype. Wing pictures were made with a Spot digital camera coupled to a Zeiss Axioplam microscope (Zeiss [Carl Zeiss], Thornwood, NY), using the 5 × and 20 × objectives for wing sizes and trichome number, respectively. Cell size was calculated from the number of trichomes in a dorsal region located between the L5 and the posterior wing margin. The number of cells was estimated as the ratio between wing size and cell size values. The nucleus size of salivary gland cells ($n = 5$) and the clone size in the wing discs ($n = 17$) were measured in pixels using the "Analyse" tool in Adobe Photoshop. We estimated clone size in the wing disc as the area occupied by all clones present in a disc. All data were collected and processed in Microsoft Excel, and analyzed using a *t*-test. We considered *P*-values < 0.001 (*** or ###), < 0.01 (** or ##), and < 0.05 (*or #) to be significant.

Microarray experiments

We compared the expression profiles of three genetic conditions: (1) *UAS-dicer2/+*; *nub-Gal4/UAS-GFP* (control discs), (2) *UAS-dicer2/+*; *nub-Gal4/UAS-Smad2^{PM}* (Smad2^{PM}), and (3) *UAS-dicer2/+*; *nub-Gal4/+*; *UAS-Smad2-RNAi/+* (Smad2i). In all experiments, the larvae were raised at 25° and the messenger RNA (mRNA) was extracted from four biological replicas for each genotype. RNA was extracted following a TRIzol protocol (TRIzol Reagent, Ambion) and posterior DNase treatment (DNA-*free* kit, Ambion) from groups of 40–80 third instar wing discs previously stored at −80° in RNA stabilization solution (RNA*later*, Ambion) until homogenization and mRNA extraction. The total amount of mRNA

varied in each replica from 2.4 to 5.1 μg. The RNA samples were sent to BIOARRAY (http://www.bioarray.es) for further processing and hybridization in Agilent arrays specifically designed for *Drosophila melanogaster* (ID 043135). We collected imaginal discs, extracted mRNA, and compared the expression profiles of genotypes 1 with 2 (*Smad2 ^{PM} vs. control*; Smad2* array) and 1 with 3 (*Smad2i vs. control*; Smad2i array). All statistical treatments were carried out in BIOARRAY using Bioconductor and the statistical packages Limma, Marray, affy, pcaMethods, and EMA, run in an R environment. In brief, the samples were analyzed by principal components analysis (PCA), and the quality of each array was checked using Feature extraction software (v10.7 from Agilent), removing nonvalid spots (outliers) and evaluating red/green (RG) densities and MA plots. Intensity data were analyzed by background subtraction (Normexp; offset of 10), intra-array normalization (Loess method), and interarray normalization (Aquantiles method). Normalized data were adjusted to a lineal model and to an empiric Bayesian model, obtaining the list of genes with differential expression showing an adjusted P-value < 0.05.

In situ hybridization

Imaginal discs were dissected and fixed in 4% formaldehyde for 30 min at room temperature, washed in PBS-0.1% Tween (PBT), and refixed for 20 min at room temperature with 4% formaldehyde, 0.1% Tween. After three washes in PBT, discs were stored at −20° in hybridization solution (SH; 50% formamide, SSC 5 ×, 100 μg/ml salmon sperm DNA, 50 μg/ml heparin, and 0.1% Tween). Discs were prehybridized for 2 hr at 55° in SH and hybridized with digoxigenin (DIG)-labeled RNA probes at 55°. The probes were previously denatured at 80° for 10 min. All the solutions used before hybridization were treated with DEPC (Sigma). After hybridization, discs were washed in SH and PBT and incubated for 2 hr at room temperature in a 1:4000 dilution of anti-DIG antibody (Roche). After incubation, the discs were washed in PBT and the detection of probes was done with 4-Nitro blue tetrazolium chloride (NBT) and 5-Bromo-4-chloro-3-indolyl-phosphate (BCIP) solution (Roche). The discs were mounted in 70% glycerol. Pictures were taken using a Spot digital camera coupled to a Zeiss Axioplam microscope using the 20 × objective. All images were processed with Adobe Photoshop CS6. RNA probes were generated using complementary DNA from the collections of Expression Sequence Tags (EST) of Berkeley *Drosophila* Genome Project, or by PCR from genomic DNA using primers with the recognition sequences of the RNA polymerase T7 (5′-TAATACGACTCACTATAGGG-3′ in the forward primer) and T3 (5′-ATTAACCCTCACTAAAGGGA-3′ in the reverse primer) in their ends (described in Table S2). The transcription to generate antisense probes was done using the RNA polymerase T7, T3, or SP6 in the presence of DIG (DIG RNA labeling mix, Roche) at 15° during 2 hr, and the probes were precipitated and suspended in H_2O DEPC. *CycE*- and S*tg*-specific RNA probes were a gift from N. Barrios and A. Baonza, respectively.

Functional annotation and Gene Ontology (GO) analysis

Microarray-selected genes were associated to GO groups based on Biological processes using the information available in FlyBase. The analysis of GO enrichment was performed using the software DAVID (Huang da *et al.* 2009). We searched for the GO term "Biological process" (GOTERM_BP) in a list of FlyBase Gene IDs for the collections of genes identified in the microarray experiments against the *D. melanogaster* genome as background. We accepted those GO terms with P-value < 0.05 as a significant enrichment.

Chromatin immunoprecipitation (ChIP)-on-chip

ChIP followed by hybridization to genome tiling arrays (ChIP-on-chip) was performed using the method described by Sandmann *et al.* (2006) with minor modifications. Three biological replicates of 150 *nub-Gal4/UAS-HA-Smad2^{PM}* wing discs each were collected, homogenized, and sonicated using a Bioruptor (Giagenode) in seven cycles of 30 sec on/30 sec off. Immunoprecipitation (IP) was carried out with 125 μl of sonicated chromatin per experiment. To assess the capability of HA-Smad2 PM to bind DNA, we used samples immunoprecipitated with an anti-HA rabbit antibody-ChIP grade (1:400; abcam9110) compared with those immunoprecipitated with anti-βGal antibody (1:4000; abcam616). All the IPs were processed for hybridization with HD2 NimbleGen tiling arrays (Roche). All raw data sets were quantile-normalized together before using the Ringo Bioconductor package for peak calling at different false discovery rates (FDRs) (Toedling *et al.* 2007). Window score (SGR) and binding interval (BED) files were visualized with the Integrated Genome Browser software (Nicol *et al.* 2009). We use R5/dm3 annotation as the *Drosophila* genome reference.

Data availability

Drosophila strains generated in this work are available upon request. All data generated or analyzed during this study are included in this published article and its supplemental files.

Results

TGFβ loss-of-function growth defects during development

TGFβ/Activin loss-of-function, caused by the expression of RNAi against different components of the pathway in the wing disc, leads to wings smaller in size (Figure 1, A and C). Complementarily, the expression of a phospho-mimic form of Smad2 (Smad2^{PM}), which simulates a constitutively active form of the protein, results in an increase in wing size (Figure 1, A and D). To better define the disc-autonomous requirement for Smad2 during wing disc development, we generated *Smad2* homozygous mutant wings (*Smad2^{F4}*) in *Smad2^{F4}* heterozygous flies (*Smad2^{F4} FRT19A/FRT19A*

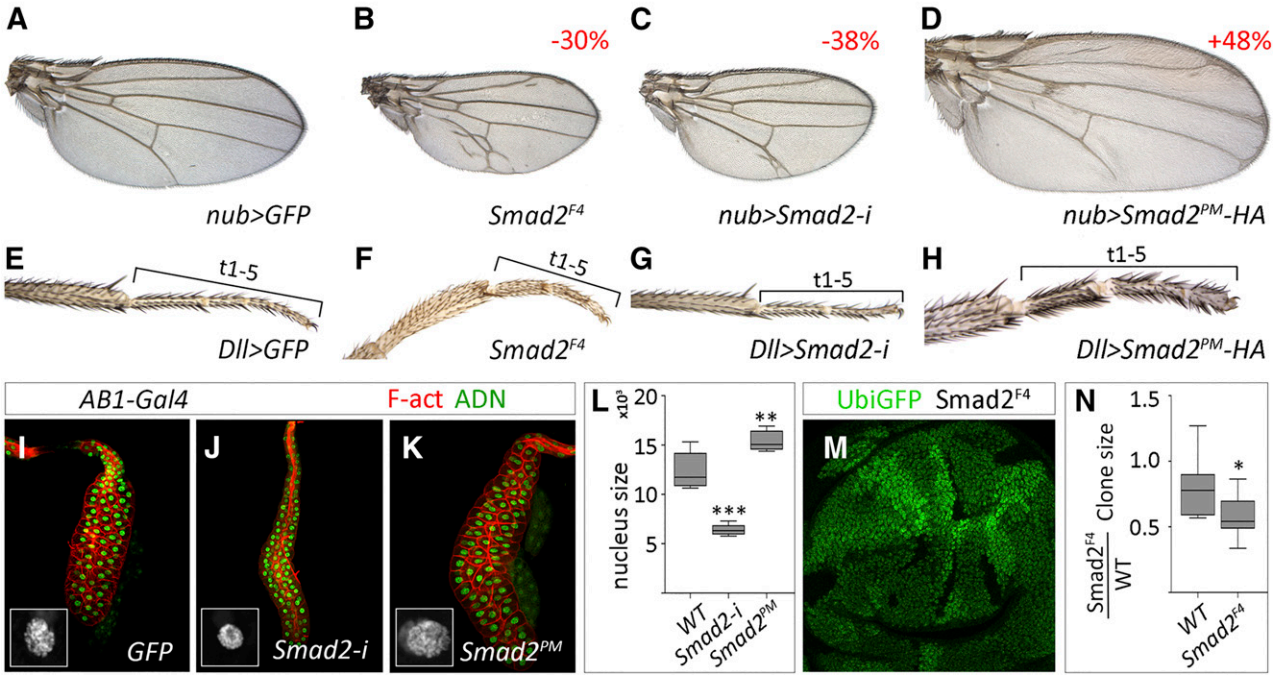

Figure 1 Phenotypic effects of altered *Smad2* expression. (A–D) Wings of *nub-Gal4 UAS-GFP/+* (control) (A), *Smad2^{F4} FRT19A/FRT19 AM(1)o^{sp}; nub-Gal4/+; UAS-FLP/+* (B), *nub-Gal4/+; UAS-Smad2-i/+* (C), and *nub-Gal4/UAS-Smad2^{PM}-HA* (D) genotypes. (E–H) Tibial and tarsal segments of *dll-Gal4/UAS-GFP* (E), *Smad2^{F4} FRT19A/FRT19 AM(1)o^{sp}; dll-Gal4 UAS-FLP/+* (F), *UAS-dicer2/+; dll-Gal4/UAS-Smad2-i* (G), and *dll-Gal4/UAS-Smad2^{PM}-HA* (H) genotypes. The tarsal segments 1–5 (t1–5) are indicated by black brackets. Loss of *Smad2* in homozygous *Smad2^{F4}* wings (B) and legs (F), or by expression of RNAi in the wing disc (C) or leg disc (G), results in smaller wings and legs. Conversely, expression of activated Smad2 in the wing or leg discs results in larger wings (D) and legs (H). (I–L) Modification of Smad2 activity in the salivary gland, a polyploid tissue, results in smaller (*AB1-Gal4/UAS-Smad2i*) (J) or larger (*AB1-Gal4/UAS-Smad2^{PM}-HA*) (K) nuclei compared to controls (*AB1-Gal4/UAS-GFP*) (I). Images were taken using the 10 × objective. White boxes (10 μm) show a 7 × magnification of the nuclei. Quantifications of nuclei size in these three genotypes are shown in (L) (n = 5). (M and N) Twin analysis of *Smad2^{F4}* cells generated in *Smad2^{F4} FRT19A/FRT19A Ubi-GFP hs-FLP1.22* wing discs. *Smad2^{F4}* homozygous cells are labeled by the absence of GFP (black) and twin wild-type cells by intense expression of GFP (green). Images were taken using the 40 × objective. The quantification of average mutant *vs.* twin clone size is shown in (N) (n = 17). DNA, ; F-act, F-actin; RNAi, RNA interference; WT, wild-type.

M(1)o^{sp}; *nub-Gal4/+*; *UAS-FLP/+*). These wings were 30% smaller than normal wings, and developed ectopic veins around the longitudinal L5 vein (Figure 1B). This observation confirms that Smad2 activity is mostly necessary for the wing to reach its normal size. The ectopic veins differentiated in Smad2i or *Smad2^{F4}* homozygous mutant wings are a consequence of ectopic Mad phosphorylation during pupal development (Sander *et al.* 2010). Altered *Smad2* function in leg discs also results in the formation of legs with abnormal size (Figure 1, E–H). We also explored the requirement of Smad2 in polyploid tissues such as the salivary glands. In this context, loss or gain of *Smad2* expression reduces or increases, respectively, nuclei size (Figure 1, I–L), suggesting that TGFβ signaling could affect endoreplication rates. These and previous results indicate that Smad2 displays growth-promoting effects in different larval tissues during *Drosophila* development.

The size defects observed upon loss of *Smad2* are not caused by gross defects in cell growth or viability, or by defects in any particular cell cycle transition, but they can be mostly attributed to a decrease in cell proliferation rates (Hevia and de Celis 2013). We examined the proliferation of *Smad^{F4}* mutant cells by clonal analysis in *Smad2^{F4} FRT19A/FRT19A Ubi-GFP hs-FLP1.22* wing discs and found that *Smad2* homozygous mutant clones are smaller than their wild-type twins (Figure 1, M and N). The reduced wing size of Smad2 mutant wings is compatible with a slower proliferation pace of mutant imaginal cells sustained during the whole development of the disc.

Smad2 combinations with cell cycle regulators

A reduced rate of cell division might be related to changes in the expression or activity of canonical regulators of cell cycle progression. We have previously shown that changes in the function of Smad2 do not cause specific defects in either the G1 to S or G2 to M cell cycle transitions (Hevia and de Celis 2013), suggesting that both steps might be affected to a similar extent. We examined the expression of two cell cycle regulators, *CycE* and *string*, in loss-of-function *Smad2* wing discs. The function of CycE is required for the G1 to S transition (Duronio *et al.* 1998), whereas the Cdc25 phosphatase String in required for the G2 to M one (Edgar *et al.* 1994). In *en-Gal4/UAS-Smad2i* wing discs, where the posterior compartments are smaller than the corresponding anterior ones, we could not detect any difference in the expression pattern or levels of *CycE* and *stg* (Figure 2, A–B'), suggesting that the

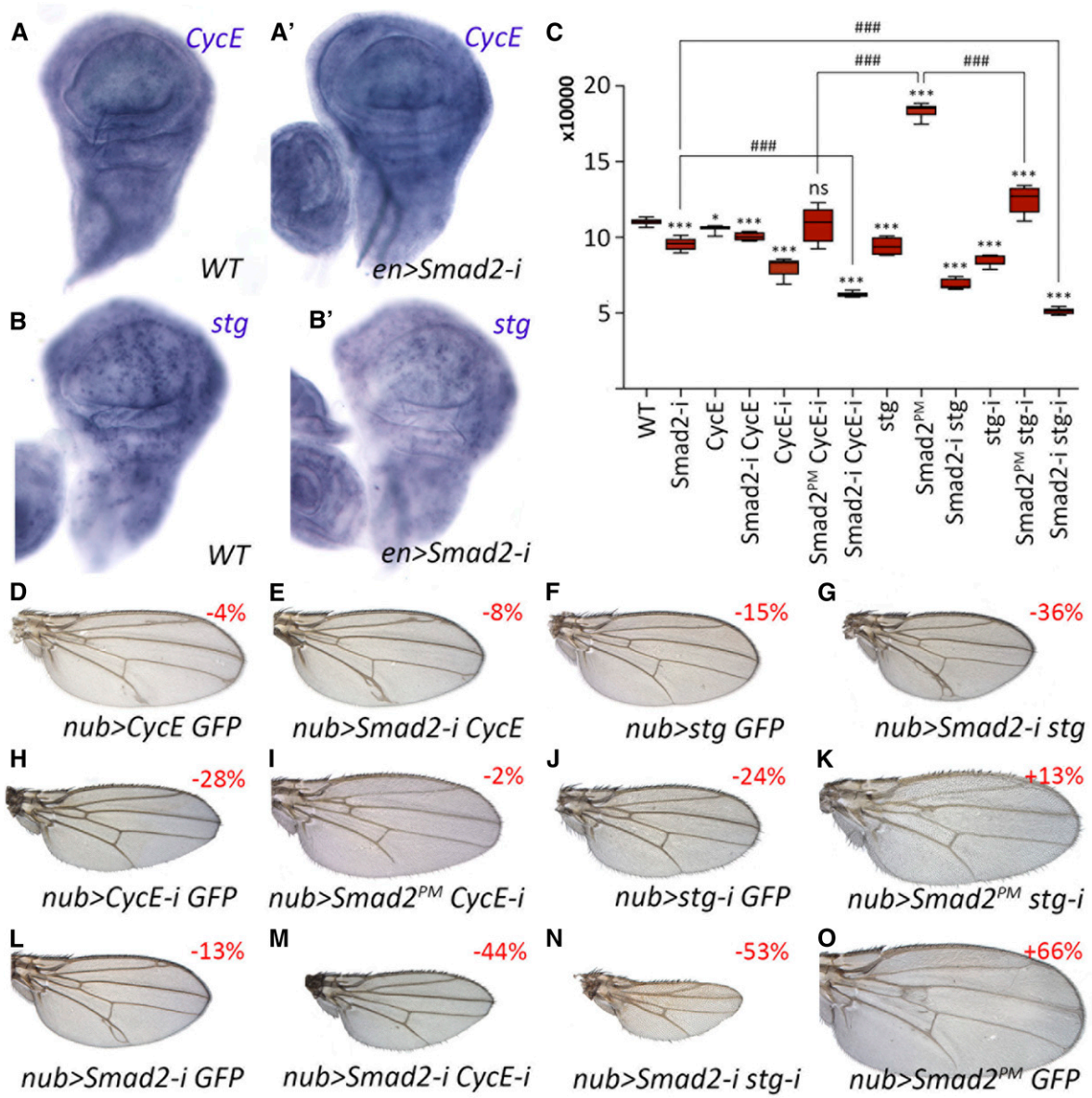

Figure 2 Genetic combinations between *Smad2* and genes regulating cell cycle progression. (A and A') Expression of Cyclin E (*CycE*) in control (WT) (A) and *en-Gal4/UAS-Smad2-i* (A') third instar wing discs. (B and B') Expression of *string* (*stg*) in control (WT) (B) and *en-Gal4/UAS-Smad2-i* (B') third instar wing discs. (C) Box plot quantification of wing size in genetic combinations between *Smad2* and *CycE* or *stg* conditions. Relevant comparisons (*t*-test; $n = 10$) are indicated by brackets with the # symbol, comparisons with WT wings are indicated by (*). We consider *P*-values < 0.001 (*** or ###), 0.01 (** or ##), and 0.05 (* or #) as significant. (D–G) Effects of *CycE* (D and E) and *stg* (F and G) overexpression on the Smad2-i phenotype. (H–K) Rescue of $Smad2^{PM}$ by reduced expression of *CycE* (H and I) and *stg* (J and K). (L) Control *Smad2-i* wing (*nub-Gal4 UAS-GFP/+*; *UAS-Smad2-i/+*). (M and N) Synergistic effects of reduced expression of *Smad2* in combination with loss of *CycE* (M) and loss of *stg* (N). (O) Control $Smad2^{PM}$ wing (*nub-Gal4 UAS-GFP/UAS-*$Smad2^{PM}$). Numbers in red indicate the percentage of wing size reduction (−) or increase (+) of mutant wings compared to their controls. WT, wild-type.

contribution of Smad2 to the regulation of *CycE* and *stg* expression is, if any, minor. On the other hand, the expression of *CycE* and *stg* is increased in *en-Gal4/UAS-*$Smad2^{PM}$ discs (Figure S1, A and B), which could be accelerating both G1–S and G2–M transitions. We also studied the phenotype of genetic combinations in which the expression of *CycE* and *stg* is modified in *Smad2i* and $Smad2^{PM}$ backgrounds. We found that the overexpression of *CycE* or *stg* does not rescue the reduction in wing size caused by the loss of *Smad2* (Figure 2, E and G, compare with controls in Figure 2, D, F, and L and quantified in Figure 2C). These results indicate that Smad2 involvement in the control of cell division cannot be explained by changes in the expression of cell cycle regulators. Complementarily, the reduction in *CycE* or *stg* expression levels is very effective in suppressing the phenotype of $Smad2^{PM}$ expression, resulting in wings of intermediate size (Figure 2, I and K, compare with controls in Figure 2, H, J, and O and quantified in Figure 2C). Furthermore, combinations involving

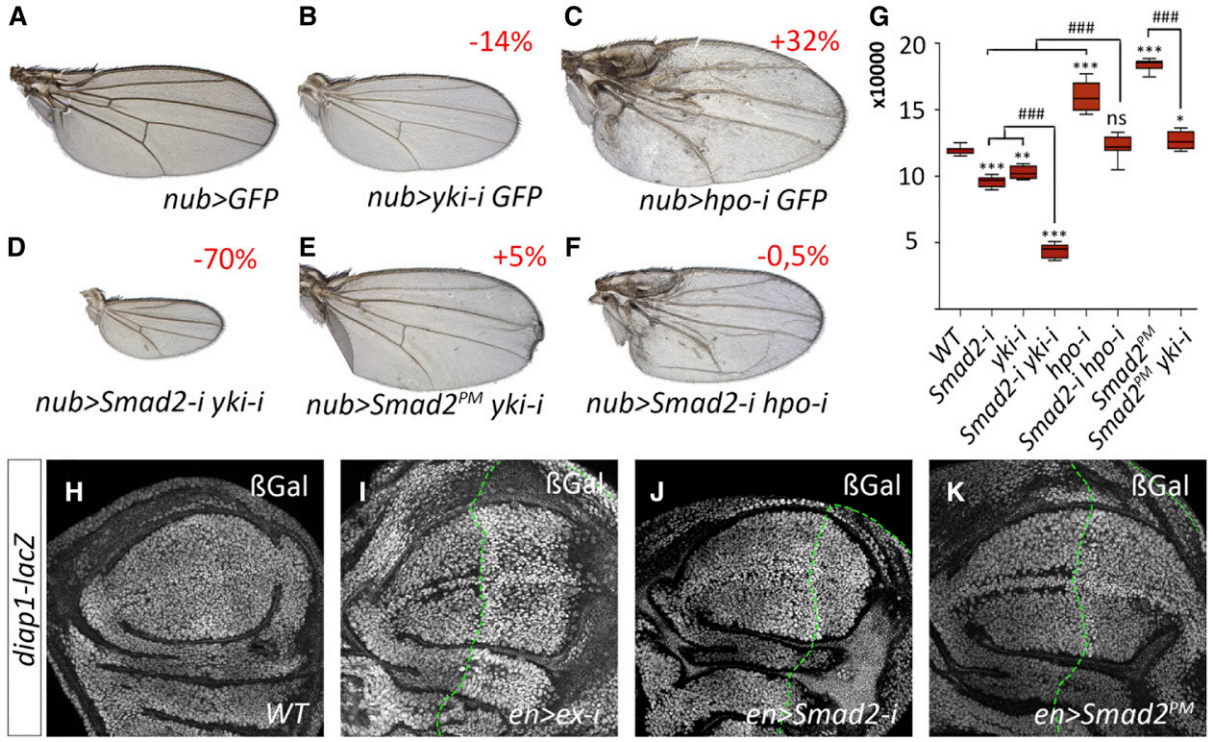

Figure 3 Genetic interactions between *Smad2* and Hippo/Yorkie (Yki) signaling. (A–C) Control wing (*nub-Gal4/UAS-GFP*) (A) and altered wing size resulting from reduced *yorkie* expression (*nub-Gal4 UAS-GFP/UAS-yki-i*) (B) or reduced Hippo signaling (*nub-Gal4 UAS-GFP/UAS-hpo-i*) (C). (D) Strong wing size reduction caused by simultaneous reduction in *yki* and *Smad2* expression (*nub-Gal4 UAS-Smad2-i/+*; *UAS-yki-i/+*). (E and F) Reciprocal normalization of wing size in *Smad2^{PM}/yki* and *hpo/Smad2* combinations (*nub-Gal4 UAS-Smad2^{PM}/+*; *UAS-yki-i/+*) (E) and *nub-Gal4 UAS-Smad2-i/+*; *UAS-hpo-i/+*) (F). Numbers in red indicate the percentage of wing size reduction (−) or increase (+) of mutant wings compared to the controls. (G) Box plot quantification of the genetic combinations shown in (A–F) and their respective controls (*nub-Gal4 UAS-GFP/+*, *nub-Gal4 UAS-GFP/UAS-Smad2i*, and *nub-Gal4 UAS-GFP/UAS-Smad2^{PM}*. Relevant comparisons (*t*-test; $n = 10$) are indicated by brackets with the # symbol, comparisons with wild-type (WT) wings are indicated by (*). We consider *P*-values < 0.001 (*** or ###), 0.01 (** or ##), and 0.05 (*or #) to be significant. Ns indicates no significant changes. (H–K) Expression of the Hippo signaling reporter *diap1-lacZ* in control discs (H), *en-Gal4 UAS-GFP/UAS-ex-i* (I), *en-Gal4 UAS-GFP /UAS-Smad2-i* (J), and *en-Gal4 UAS-GFP /UAS-Smad2^{PM}* (K). The expression of *diap1-lacZ* (gray) in the posterior compartment of the wing disc (green line) is only modified when Hippo signaling is reduced (I).

loss of *Smad2* in genetic backgrounds of reduced *CycE* or *stg* expression result in stronger phenotypes of reduced wing size (Figure 2, M and N; quantified in Figure 2C). These results suggest that cell cycle regulators participate in the generation of Smad2 phenotypes, but they do not seem to correspond to primary targets of Smad2 regulation.

Smad2 interactions with the HSW signaling pathway

The HSW signaling pathway is a key regulator of imaginal disc growth, and several links between this pathway and TGFβ signaling have been already described (Varelas *et al.* 2008; Oh and Irvine 2011). We first analyzed possible functional interactions between these two pathways by making genetic combinations between gain- and loss-of-function conditions in each pathway. As expected, knockdown of *yorkie* (*yki*), the HSW pathway transducer, or *hippo* (*hpo*) in the wing disc results in the formation of smaller and larger wings, respectively (Figure 3, A–C; quantified in Figure 3G). We found that loss of *Smad2* expression reduces the overgrowth phenotype of loss of HSW signaling (Figure 3, F and G). Similarly, the reduction of *yki* expression reduces the extra growth caused by the expression of activated Smad2 (Figure 3, E and G). The phenotypes of *Smad2-i/hpo-i* and *Smad2^{PM}/yki-i* combinations are intermediate compared to the phenotypes caused by individual modifications to each pathway (Figure 3G). When we combined mutant conditions that individually reduce wing size (*Smad2-i* and *yki-i*), we found a strong synergistic effect of reduced wing size (Figure 3, D and G). We also searched for possible effects of Smad2 activity on the expression of the Yki target *diap1* (Figure 3, H–K). As expected, the reduction in HSW signaling causes a strong increase in *diap1-lacZ* expression (Figure 3I). In contrast, the expression of *diap1-lacZ* is not modified upon loss of *Smad2* or by the expression of its activated form (Figure 3, J and K). The same results were observed using other known Yki target genes such as *expanded* (*ex*; Figure S1, F–H) or Myc (Figure S1I). These results suggest that Smad2 function is not required for the expression of these HSW targets, and are compatible with Smad2 and Yki regulating independent set of genes related to the control of cell proliferation.

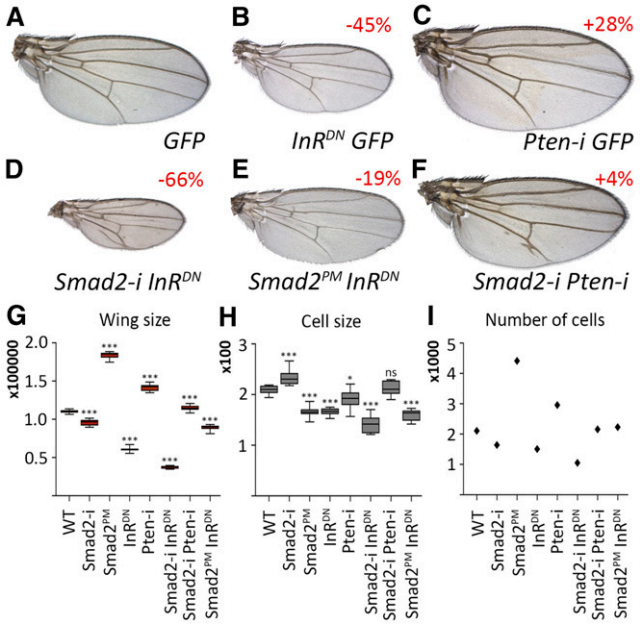

Figure 4 Genetic interactions between Smad2 and insulin receptor (InR) signaling. (A–C) Control wing (*nub-Gal4 UAS-GFP/+*) (A) and wings with reduced (*nub-Gal4 UAS-GFP/+ UAS-InR^{DN}/+*) (B) or increased (*nub-Gal4 UAS-GFP/+ UAS-pten-i/+*) (C) insulin signaling. Numbers in red indicate the percentage of wing size change comparing mutant wings to their respective controls [reduction (−) or increase (+)]. (D) Synergistic wing size reduction observed when both InR signaling and *Smad2* expression are reduced in the wing blade (*nub-Gal4/+; UAS-Smad2-i/UAS-InR^{DN}*. (E and F) Mutual phenotypic correction upon opposing changes in Smad2 activity and InR signaling in *nub-Gal4/UAS-Smad2^{PM}; UAS-InR^{DN}/+* (E) and *nub-Gal4/+; UAS-Smad2-i/UAS-pten-i* (F) wings. (G–I) Box plot quantification of wing size (G), cell size (H), and number of cells (I) in the genetic combinations shown in (A–F). Comparisons with wild-type (WT) wings (*t*-test; $n = 10$) are indicated by (*). We consider *P*-values < 0.001 (***), 0.01 (**), and 0.05 (*) to be significant. Ns indicates no significant changes.

Smad2 interactions with the insulin signaling pathway

Changes in Smad2 activity have effects not only on wing size, but also on the size of the cells (Hevia and de Celis 2013). Another pathway with significant effects on cell division and growth is InR signaling (Britton *et al.* 2002). We analyzed the possibility of functional interactions between Smad2 and InR signaling by means of genetic combinations. Loss and excess of InR signaling in the wing disc resulted in the formation of smaller and larger wings, respectively, and these wings also displayed changes in cell size and cell number (Figure 4, A–C and G–I). Loss of *Smad2* and excess InR signaling suppressed each other's phenotypes, resulting in wings of almost normal size (Figure 4, F and G–I). Similarly, in combinations involving loss of InR signaling and excess Smad2 activity, the resulting wings display intermediate sizes (Figure 4, E and G–I). The only synergistic interaction that we found involves a reduction in both *Smad2* expression and InR signaling, where the resulting wings have much smaller size that those in which only one pathway is affected (Figure 4, D and G–I). In all combinations tested, the cell size phenotypes were additive (Figure 4H). Thus, and as observed for Smad2/HSW, it seems that TGFβ and InR signaling act independently of each other on cell proliferation in the wing disc.

Search for TGFβ signaling targets in the wing disc using expression microarrays

As a complementary and unbiased approach to identify the mechanisms and genes involved in TGFβ function during imaginal disc growth, we compared the expression profile of wing discs in which the activity of Smad2 was modified. We expected that genes transcriptionally regulated by Smad2 might play a significant role in cell proliferation during imaginal development. We used loss-of-function (*UAS-dicer2/+; nub-Gal4/UAS-Smad2-RNAi*) and gain-of-function (*UAS-dicer2/+; nub-Gal4/UAS-Smad2^{PM}*) genotypes, and compared their expression profiles with control discs (*UAS-dicer2/+; nub-Gal4/UAS-GFP*). We reasoned that the expression level of individual Smad2 target genes might be modified in opposite manners in the loss- and gain-of-function conditions, as they affect wing size in opposite ways. We identified a total of 1561 genes for which expression level varied significantly in either Smad2^{PM} (Smad2^{PM} *vs.* control) or Smad2i arrays (Smad2i *vs.* control) (Figure 5A and Table S3). To further characterize these genes, it was necessary to define a reduced number of candidates; consequently we restricted all additional analyses to genes displaying a fold change > 2 (93) and to those genes whose expression levels varied in both Smad2^{PM} and Smad2i arrays (107). The 200 genes in this group has a wide variety of biological functions including cell signaling, metabolism, development-related processes, and nonannotated CG genes (Figure S2 and Table S4). The GO descriptions associated with metabolism and nervous system-related processes were the most significantly enriched within the 200 microarray-selected genes (Figure S2B).

To reduce this group of 200 genes to the most relevant candidate Smad2 target genes mediating the biological functions of the pathway, we used several complementary approaches (Figure 5). On one hand, we studied the expression pattern of these genes by *in situ* hybridization in wild-type imaginal wing discs, and also in imaginal discs in which the activity of Smad2 was modified only in the posterior compartment (*UAS-dicer2/+; en-Gal4/UAS-Smad2-i* and *en-Gal4/UAS-Smad2^{PM}*; Figure 5B). We also studied the loss-of-function phenotype of these genes (Figure 5C). In addition, we made genetic combinations between most UAS-RNAi and Smad2^{PM}, aiming to identify genes required for the overgrowth caused by the expression of Smad2^{PM} in the wing disc (Figure 5D).

Expression patterns of candidate Smad2 targets in wild-type and Smad2 mutant conditions

The expression of candidate Smad2 targets falls into the following general categories. The most numerous (63.5% of genes) includes genes expressed in a generalized manner in the wing disc ("G" in Figure 6, A and F). In addition, a

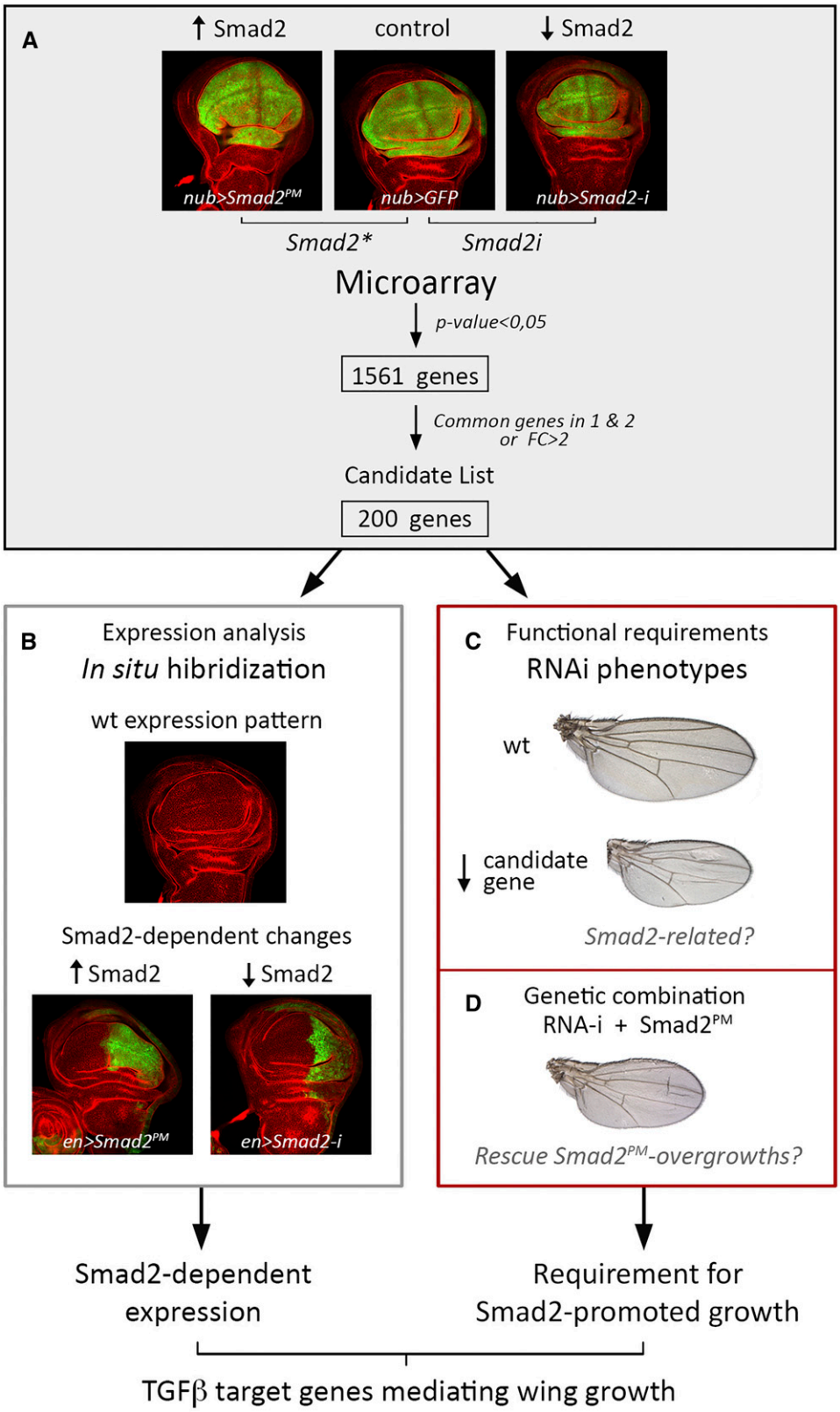

Figure 5 Experimental logic of the microarray experiments and functional approaches carried out to identify candidate Smad2 target genes. (A) Microarray experiments were carried out in wing discs of the following genotypes: *UAS-dicer2/+*; *nub-Gal4/UAS Smad2^{PM}* (right), *UAS-dicer2/+*; *nub-Gal4/UAS-GFP* (middle), and *UAS-dicer2/+*; *nub-Gal4/+*; *UAS-Smad2-i/+* (left). The expression of GFP is in green and the expression of Phaloidin in red. Below are indicated the number of identified genes in the two comparisons (1561) and the number of selected candidate genes (200). (B) Expression analysis was carried out in wing discs of the following genotypes: WT (up), *en-Gal4 UAS-GFP/ UAS-Smad2^{PM}* (bottom left), and *UAS-dicer2/+*; *en-Gal4 UAS-GFP/+*; *UAS-Smad2-i/+* (bottom right). The expression of GFP is in green and the expression of Phaloidin in red. (C) Analysis of functional requirements during wing development. The loss-of-function phenotype of most genes included in the "candidate" list was analyzed in *UAS-dicer2/+*; *nub-Gal4/ UAS-RNAi* and *UAS-dicer2/+*; *sal^{EPv}-Gal4/ UAS-RNAi* genetic combinations. Most RNAis were also tested for their ability to suppress the large wing size phenotype of Smad2^{PM} expression in *nub-Gal4 UAS-Smad2^{PM}/UAS-RNAi* combinations (D). Fold change, ; RNAi, RNA interference; WT, wild-type.

smaller number of genes (13.5%) are also expressed in most wing disc cells, but their levels of expression are consistently low ("weak generalized"; wG in Figure 6, B and F). For these two classes (G and wG), the expression coincides with the domain of activation of Smad2, which is generalized in the wing disc. A smaller fraction of genes (5.5%) were expressed in spatially restricted patterns ("P" in Figure 6, D and F) that in general were related to the developing sensory organs,

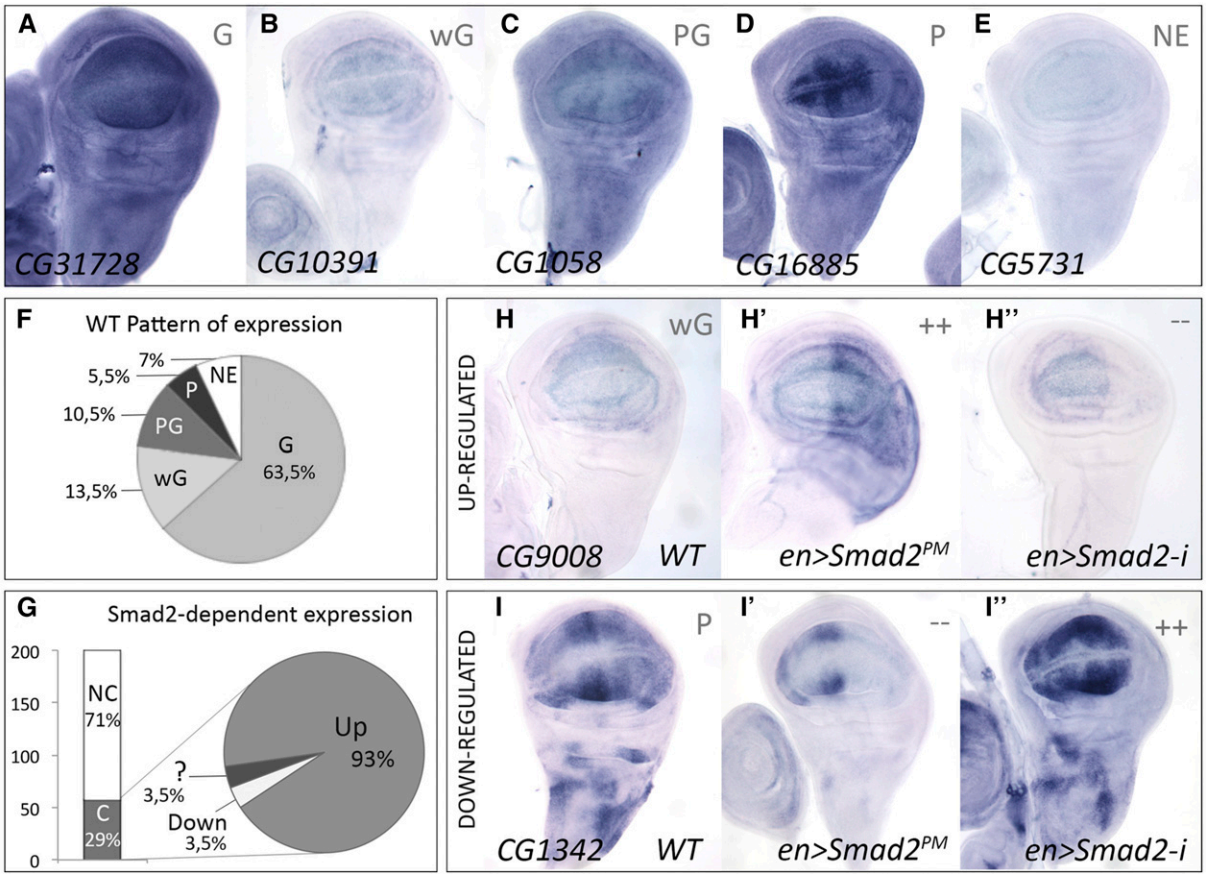

Figure 6 *In situ* hybridization of candidate Smad2 target genes. (A–E) Representative examples of *in situ* expression patterns of candidate Smad2 target genes in third instar wing discs. Generalized (G) expression pattern (*CG31728*) (A), weak generalized (wG) expression (*CG10391*) (B), generalized expression with accumulation in certain domains (PG, *CG1058*) (C), expression increased in a pattern in the wing blade (P, *CG16885*) (D), and lack of expression in the wing disc (NE, *CG5731*) (E). (F) Percentage of genes in each class of expression pattern. (G) Numerical representation of the changes in expression observed in *Smad2* mutant discs. "C" and "NC" correspond to genes in which expression changes (C) or is not modified (NC) in either *en-Gal4/UAS-Smad2^{PM}* or *UAS-dicer2/+*; *en-Gal4/UAS-Smad2-RNAi*. The circle represents the fraction of genes in which expression is upregulated (Up), downregulated (Down), or changes in the same way in *Smad2* and gain-of-function conditions (?). (H–H'') Example of *in situ* expression of a gene (*CG9008*) upregulated by Smad2, in wild-type (WT) discs (H), *en-Gal4/UAS-Smad2^{PM}* (H'), and *en-Gal4/UAS-Smad2-RNAi* (H''). (I–I'') Example of *in situ* expression of a gene (*CG1342*) downregulated by Smad2, in WT discs (I), *en-Gal4/UAS-Smad2^{PM}* (I'), and *UAS-dicer2/+*; *en-Gal4/+*; *UAS-Smad2-RNAi/+* (I'').

veins, wing margin, or wing compartments. Other genes (10.5%) were expressed in all wing disc cells but, superimposed on this generalized expression, the transcripts accumulated at higher levels in particular wing disc domains ("PG" in Figure 6, C and F). Finally, for 7% of genes, we could not identify any signal in wing discs, indicating that they are expressed below our detection threshold or not expressed at all in this tissue ("NE" in Figure 6, E and F).

The most frequent expression pattern that we found for the selected genes is compatible with them being regulated by TGFβ/Smad2, as the pathway is activated in all wing disc cells (Hevia and de Celis 2013). To visualize the transcriptional effects of Smad2 over the expression of the selected genes in the wing disc, we carried out *in situ* hybridization analysis in discs where the expression or activity of this protein was modified only in the posterior compartment (see Figure 5B). We found clear changes in expression levels in the posterior compartment of *UAS-dicer2/+*; *en-Gal4/+*; *UAS-Smad2-i/+* or *en-Gal4/UAS-Smad2^{PM}* in 29% of the analyzed cases. For most of them (93%), the regulation exerted by Smad2 was positive, because the expression levels were increased ("+" in Table 1 and Table S4) in *Smad2^{PM}* and/or reduced in *Smad2i* ("−" in Table 1 and Table S4) posterior compartments (Figure 6G). One example of a gene whose expression is activated by Smad2 is shown in Figure 6, H–H". A minority of genes (3.5%) exhibited the opposite behavior: a negative regulation (downregulation) in response to changes in Smad2 expression (Figure 6, G and I–I"). The complete results for all cases examined are shown in Figure S3, Figure S4, Figure S5, Figure S6, Figure S7, Figure S8, and Figure S9.

We found a poorer than expected correlation between microarray data and *in situ* hybridization results, and decided to focus in the group of genes that showed a clear-cut change in their *in situ* expression in the disc (Table 1). This group of 57 genes constitute a reasonable collection of candidate Smad2-regulated genes in the wing disc, and encode proteins related to developmental processes or neurogenesis

Table 1 Most relevant selected genes by *in situ* hybridization and phenotypic analysis

Gene		Array	logFC		*In situ*			Chip	Phenotype		GO	N
					wt	*	*i*		RNAi	Resc		
CG10391	Cyp310a1	+Smad2*/−Smad2i	−1.01	1.32	wG	+	−	FDR25	wt	R	Sig, Met (RedOx)	13
CG11221	CG11221	+Smad2*/−Smad2i	−0.34	0.32	G	+	=	—	F//S-V^{-}	R	CG	
CG12399	Mad	+Smad2*/−Smad2i	−2.05	0.32	G	+	=	—	sS-P	R	Sig, Dev (w), Loc	
CG9008	CG9008	+Smad2*/−Smad2i	−1.53	0.55	wG	++	−	—	PL//wS-V^{+}	R	Org, Met (C)	
CG1058	rpk	+Smad2*	−1.14	—	PG	+	=	—	S	R	Tra	
CG42281	bun	+Smad2*	−1.09	—	G	+	=	FDR10	S	R	Div, Dev, Apo	
CG6737	Vha16-5	+Smad2*	−2.98	—	G	+	=	—	S/Bs	R	Tra	
CG8420	CG8420	−Smad2i	—	1.11	wG	=	—	FDR1	S/Bs	R	CG	
CG18473	CG18473	+Smad2i	—	−1.54	G	+	=	FDR5	S	R	Met	
CG6434	CR6434	+Smad2i	—	−2.06	G	=	—	—	S	R	Sig	
CG10089	CG10089	−Smad2*/−Smad2i	0.35	0.47	G	+	=	FDR1	V^{+}	R	Sig	
CG1966	Acf1	−Smad2*/−Smad2i	1.44	1.17	G	+	—	FDR25	S	R	Dev, Neu, Met (ARN)	
CG42677	wb	−Smad2*/−Smad2i	0.45	0.34	PG	+	=	FDR25	Bs/S/F	R*	Dev, MM, Loc, Adh	
CG18657	NetA	+Smad2*/−Smad2i	−0.71	0.51	P	+	=	FDR1	S/Bs	R	Neu, Loc	4
CG16885	CG16885	+Smad2*	−1.42	—	P	+	—	—	PL//S-P	R	CG	
CG18349	Cpr67Fa2	+Smad2*	−1.22	—	P	++	—	—	S/V^{+}	R	Dev	
CG1342	Spn100A	−Smad2*/−Smad2i	1.01	1.55	P	−	++	FDR1	wS	Rp	CG	
CG11409	CG11409	+Smad2*/−Smad2i	−0.28	0.31	G	+	=	FDR1	sF//wt	NR	CG	38
CG14257	CG14257	+Smad2*/−Smad2i	−0.48	0.87	G	+	=	FDR5	wt	NR	CG	
CG15545	CG15545	+Smad2*/−Smad2i	−0.56	1.21	G	+	=	FDR5	NT	NT	CG	
CG31728	l(2)k05911	+Smad2*/−Smad2i	−0.47	0.47	G	+	—	—	NT	NT	CG	
CG4610	CG4610	+Smad2*/−Smad2i	−0.59	0.46	wG	+	=	FDR25	sF//wt	NT	ARN	
CG5836	SF1	+Smad2*/−Smad2i	−0.42	0.42	G	+	=	FDR25	NT	NT	Dev, MM, Neu	
CG6055	CG6055	+Smad2*/−Smad2i	−1.68	0.62	PG	++	−	FDR10	wt	NR	CG	
CG8246	Poxn	+Smad2*/−Smad2i	−0.74	0.49	G	+	=	—	wt	NT	Dev, MM, Neu	
CG9614	pip	+Smad2*/−Smad2i	−0.45	0.74	wG	=	—	FDR10	wt	NT	Sig, Dev	
CG11594	CG11594	+Smad2*	−1.84	—	wG	=	—	FDR1	wt	NR	Met (C)	
CG12370	Dh44-R2	+Smad2*	−1.33	—	G	+	=	—	wt	NR	Sig, Def	
CG12688	CG12688	+Smad2*	−1.00	—	G	+	=	—	sF//wt	NR	CG	
CG15444	ine	+Smad2*	−1.08	—	G	+	—	FDR5	wt	NR	Dev, Sig, Neu	
CG18294	CG18294	+Smad2*	−1.42	—	G	+	=	—	NT	NT	CG	
CG2052	dati	+Smad2*	−1.83	—	G	+	=	FDR5	wt	NR	Neu, Dev	
CG32368	CG32368	+Smad2*	−1.83	—	G	+	=	—	wt	NT	CG	
CG34002	CG34002	+Smad2*	−1.57	—	G	+	=	—	NT	NT	CG	
CG6485	ND-24L	+Smad2*	−1.75	—	G	++	=	FDR5	wt	NR	Met (RedOx)	
CG7328	CG7328	+Smad2*	−1.37	—	G	+	=	—	wt	NT	Met (C)	
CG9328	CG9328	+Smad2*	−1.33	—	wG	+	—	FDR25	wt	NR	CG	
CG15236	CG15236	−Smad2i	—	1.03	G	+	=	FDR25	Bs/S	NT	CG	
CG1139	CG1139	−Smad2i	—	1.13	NE	++	=	FDR5	wt	NT	Tra, Div	
CG12224	CG12224	+Smad2i	—	−1.70	G	+	=	FDR25	wt	NR	Met (RedOx)	
CG13032	CG13032	+Smad2i	—	−1.73	wG	++	=	FDR25	wt	NR	CG	
CG8687	Cyp6a14	+Smad2i	—	−1.62	G	+	=	—	NT	NT	Met (RedOx)	
CG9118	LysD	+Smad2i	—	−2.51	G	+	=	—	sF//wt	NR	Def	
CG12972	ebd2	+Smad2*/+Smad2i	−0.38	−0.35	G	=	+	FDR10	wt	NT	Dev	
CG14025	Bsg25D	+Smad2*/+Smad2i	−0.35	−0.36	G	+	=	—	sF//wt	NR	CG	
CG16800	CG16800	+Smad2*/+Smad2i	−1.35	−0.81	G	+	=	—	wt	NR	CG	
CG1851	Ady43A	+Smad2*/+Smad2i	−1.21	−0.73	G	+	+	—	wt	NT	Met	
CG18543	mtrm	+Smad2*/+Smad2i	−0.66	−0.41	G	+	+	FDR25	wt	NT	Div	
CG43161	Skeletor	+Smad2*/+Smad2i	−0.58	−0.48	G	+	=	FDR25	wt	NR	Div	
CG4920	ea	+Smad2*/+Smad2i	−1.57	−1.59	G	+	=	—	wt	NR	Sig, Def	
CG6665	CG6665	+Smad2*/+Smad2i	−0.26	−0.38	G	+	=	FDR25	wt	NR	CG	
CG7173	CG7173	+Smad2*/+Smad2i	−1.28	−1.45	G	+	=	—	wt	NT	CG	
CG13707	CG13707	−Smad2*/−Smad2i	0.45	1.26	G	+	=	FDR5	wt	NT	CG	
CG5497	mRpS28	−Smad2*/−Smad2i	1.76	0.64	G	+	=	—	F/Nec	NT	Org, ARN	
CG7607	CG7607	−Smad2*/−Smad2i	0.59	1.38	G	=	—	FDR10	wt	NR	CG	
CG8084	ana	+Smad2*/−Smad2i	−2.10	1.16	P	++	−	FDR1	wt	NR	Neu, Div	2
CG7941	Cpr67Fa1	+Smad2*	−2.22	—	P	+	—	—	NT	NT	Dev	

(continued)

Table 1, *continued*

Gene		Array	logFC		*In situ*			Chip	Phenotype		GO	N
					wt	*	*i*		RNAi	Resc		
CG5792	Pih1D1	+Smad2*/−Smad2i	−0.35	0.39	G	=	=	FDR25	S/V$^+$	Rp	CG	27
CG15152	CG15152	+Smad2*	−1.61	—	G	=	=	FDR5	S/F	R	CG	
CG15212	CG15212	+Smad2*	−1.13	—	PG	=	=	—	S	R	CG	
CG32318	CG32318	+Smad2*	−3.09	—	G	=	=	—	nW//sS-P	R	Cyt	
CG32581	CG32581	+Smad2*	−4.67	—	G	=	=	FDR25	PL//wS-wV$^+$	Rp	CG	
CG43646	CG43646	+Smad2*	−1.82	—	G	=	=	—	NT	NT	CG	
CG10719	brat	−Smad2i	—	1.02	G	=	=	—	wS/Bs	Rp	Tra, Sig, Neu, Loc	
CG31436	CG31436	−Smad2i	—	1.55	G	=	=	FDR1	S-V$^-$	Rp	CG	
CG3649	CG3649	−Smad2i	—	1.03	P	=	=	FDR25	sS-P//S-wP	Rp	Tra	
CG6646	DJ-1alpha	−Smad2i	—	1.16	G	=	=	—	wS	Rp	Met (RedOx)	
CG7106	lectin-28C	−Smad2i	—	1.54	wG	=	=	—	N	R**	CG	
CG12366	O-fut1	−Smad2*/+Smad2i	0.41	−0.41	G	=	=	—	sN/nW//N/S	R*	Sig, Met, Neu	
CG32491	mod(mdg4)	−Smad2*/+Smad2i	0.27	−0.25	G	=	=	FDR5	S/wF	R	Div, Loc, Apo	
CG14692	CG14692	+Smad2i	—	−1.62	wG	=	=	FDR25	S	Rp	Sig	
CG17533	GstE8	+Smad2i	—	−1.19	G	=	=	—	PL/nW//wS	Rp	Met (C)	
CG17599	CG17599	+Smad2i	—	−1.22	G	=	=	FDR1	sS	R	Cyt	
CG8129	CG8129	+Smad2i	—	−1.62	wG	=	=	FDR25	wS	Rp	Met	
CG18066	Cpr57A	+Smad2*/+Smad2i	−1.78	−1.09	NE	=	=	—	S/wF	R	Dev	
CG18455	Optix	+Smad2*/+Smad2i	−1.00	−0.77	P	=	=	FDR10	wS-P	Rp	Dev, Neu, Sig	
CG3616	Cyp9c1	+Smad2*/+Smad2i	−1.02	−0.33	wG	=	=	FDR10	S	R	Met (RedOx)	
CG5313	RfC3	+Smad2*/+Smad2i	−0.32	−0.58	wG	=	=	—	S-P	R**	Neu, Sig	
CG9733	CG9733	+Smad2*/+Smad2i	−0.63	−1.58	PG	=	=	FDR25	PL//sS-P	R	Def	
CG12182	CG12182	−Smad2*/−Smad2i	0.46	0.81	G	=	=	FDR25	sS-P	R	CG	
CG13083	CG13083	−Smad2*/−Smad2i	1.54	1.54	G	=	=	—	PL/nW//S	Rp	CG	
CG2849	Rala	−Smad2*/−Smad2i	2.74	2.57	wG	=	=	FDR5	nW//sS-P	R	Neu, Dev, Sig, Met, Def	
CG4103	THG	−Smad2*/−Smad2i	0.77	0.56	G	=	=	—	PL//F	R	Tra	
CG9333	Oseg5	−Smad2*/−Smad2i	2.11	1.25	G	=	=	FDR10	sS/V$^+$	Rp	Cyt	

Genes with confirmed *in situ* hybridization changes in Smad2 mutant discs (38 genes ubiquitously expressed and two genes showing a restricted pattern of expression), in which loss-of-function rescues Smad2^{PM} promoted overgrowth ($N = 27$), and fulfilling both criteria (13 genes ubiquitously expressed and 4 genes showing a restricted pattern of expression). Array columns show the array where each gene was identified and the logFC values: Smad2* corresponds to the microarray that compared Smad2^{PM} *vs.* control and −Smad2i compared Smad2-i *vs.* control. + and − indicate that the expression level increased or decreased, respectively, in mutant *vs.* control situations. *In situ* columns indicate the pattern of expression of each gene in wild-type (*wt*), *en-Gal4 UAS-GFP/UAS-Smad2^{PM}* (*), and UAS-dicer2/+; *en-Gal4 UAS-GFP/+*; *UAS-Smad2-RNAi/+* (*i*) discs: generalized expression (G), weak generalized expression (wG), generalized expression with a higher accumulation in certain domains (PG), expression restricted to a pattern (P), and lack of expression (NE). +, −, and = symbols indicate an increase, decrease, or no detectable change in the expression in the posterior mutant compartment compared with anterior, respectively. Chip column shows the genes where we detected peaks by ChIP-on-chip at different false discovery rates (FDR1, 5, 10, and 25). Phenotype RNAi column indicates the consequence of downregulating each gene using RNAi expressed with *nub-Gal4* or *sal^{EPv} drivers* (nub//sal): size defects (S), size combined with pattern defects (S-P), ectopic veins (V$^+$), loss of veins (V$^-$), blistered wings (Bs), folded wings (F), phenotype-related with Notch defects (N), necrosis (Nec), nW (no wing), lethality in pupal stage (PL), no defects (wt), and not tested (NT). "s" and "w" mean strong and weak phenotypes, respectively. Resc column represents the result of combining each RNAi with the expression of Smad2^{PM}: rescue of Smad2^{PM} overgrowth (R), partial rescue (Rp), no rescue (NR), synergistic phenotype (R*), or not tested (NT). GO column indicates the gene ontology (GO) terms based in biological processes (BP) associated to each gene in FlyBase. We grouped the BP terms in the following categories: signaling and regulation of transcription (Sig), transport (Tra), developmental and morphogenetic processes (Dev), cell adhesion (Adh), metabolism [Met; including reduction/oxidation (RedOx), carbohydrates (C), proteins (P), and others), defense or immune response (Def), nervous system-related processes (Neu), cell division (Div), apoptosis (Apo), locomotion (Loc), cytoskeleton organization (Cyt), metamorphosis (MM), subcellular components organization (Org), or genes with no annotated functions (CG).

(14 genes), metabolism (eight genes), cell division (three genes), transport (three genes), signaling (seven genes), and genes without assigned function (22 CG genes).

Phenotypic analysis of candidate Smad2 target genes

We expected that genes regulated by Smad2 in the wing disc might be involved in the implementation of its growth-promoting function, and consequently that a reduction in their expression would result in the formation of smaller than normal wings. To identify the functional requirements of candidate Smad2 targets, we expressed RNAi for each of the microarray-selected genes in the wing disc (Figure 7, Figure S10, Figure S11, and Figure S12). A fraction of these 200 genes (30%) displayed a loss-of-function phenotype in the wing (Figure 7D). The most frequent phenotype consisted of a reduction of wing size (76%), including those cases where the only effect was on wing size ("S"; 40%; Figure 7, B and E and Figure S10) and those in which wing size reduction was accompanied by severe alterations in the venation pattern ("S-P"; 36%; Figure 7, C and F and Figure S11). Other phenotypes that we identified were unrelated to the known requirements of Smad2, and included blistered wings ("Bs"; Figure 7G), defects in the wing margin, and vein thickening ("N"; Figure S12). Representative examples of wing size phenotypes, with or without associated pattern defects, are shown in Figure 7, B–G, and the complete collection of phenotypes is presented in Figure S10, Figure S11, and Figure S12 grouped by phenotypic class.

As an additional test to determine whether the selected genes implement the function of Smad2, we crossed the RNAi for all the genes whose phenotype consisted of wing size

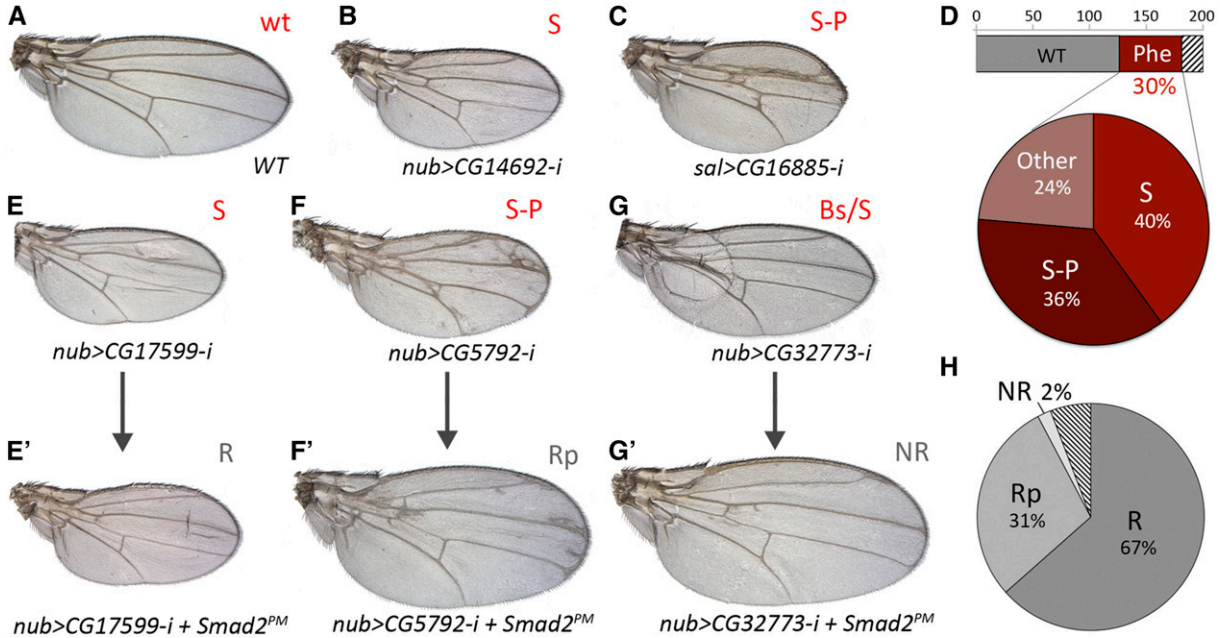

Figure 7 Phenotypic analysis of candidate Smad2 target genes. (A) Wild-type (WT) wing. (B and C) Representative examples of wings expressing RNA interference (RNAi) of *CG14692* (*UAS-dicer2/+*; *nub-Gal4/UAS-CG14692-RNAi*) (B) and *CG16885* (*UAS-dicer2/+*; *sal^{EPv}-Gal4/UAS-CG16885-RNAi*). These wings show reduced size and normal pattern (class S in red) (B) and reduced size and altered pattern of veins (class S-P in red) (C). (D) Number of genetic combinations tested resulting in normal wings (gray bar, WT) or altered wings (red bar, Phe). Not tested genes are represented by striped bar. The circular sectors represent the distribution of phenotypic classes including wing size (S), wing size and vein pattern (S-P), and other (Other) phenotypes including blistered wings, Notch-like phenotype of vein thickening, or wing margin loss and alterations in epithelial integrity or wing pigmentation. (E and E') Representative example of suppression of the Smad2^{PM} phenotype by the expression of *CG17599* RNAi (*UAS-dicer2/+*; *nub-Gal4 UAS-Smad2^{PM}/UAS-CG17599-RNAi*) (E'), and control wing of *UAS-dicer2/+*; *nub-Gal4 UAS-GFP/UAS-CG17599-RNAi* genotype (E). (F and F') Representative example of partial suppression of the Smad2^{PM} phenotype by the expression of *CG5792* RNAi (*UAS-dicer2/+*; *nub-Gal4 UAS-Smad2^{PM}/UAS-CG5792-RNAi*) (F'), and control wing of *UAS-dicer2/+*; *nub-Gal4 UAS-GFP/UAS-CG5792-RNAi* genotype (F). (G and G') Representative example of Smad2^{PM} phenotype unaffected by the expression of CG32773 RNAi (*UAS-dicer2/+*; *nub-Gal4 UAS-Smad2^{PM}/UAS-CG32773-RNAi*) (G') and control wing of *UAS-dicer2/+*; *nub-Gal4 UAS-GFP/UAS-CG32773-RNAi* genotype (G). Results of genetic combinations between RNAi of candidate genes and Smad2^{PM} expression. Total rescue of the Smad2^{PM} phenotype (R, see example in (E')), partial rescue (Rp; see example in (F')), lack of effects (NR; see example in (G')), and nontested cases (striped section).

defects (n = 49) into a Smad2^{PM} background. We expected that, if these genes participated in Smad2 function, the reduction in their expression should correct the large wing size caused by the overexpression of Smad2^{PM}. We grouped the results into the following categories. The majority of genes tested were able to entirely ("R"; 67%) or partially ("Rp"; 31%) suppress the Smad2^{PM} overexpression phenotype (Figure 7, E'–F' and H). We included these 27 genes as candidates to mediate the function of Smas2 during wing disc growth (Table 1). These genes encode proteins involved in metabolism (five genes), signaling (four genes), development or neurogenesis (three genes), cytoskeleton organization (three genes), transport (four genes), and nonassigned genes (eight CG genes). In two cases, *CG10089* and *CG10391*, the reduction of their expression did not affect wing size, but it was able to suppress the extra growth of wings expressing activated Smad2 (Figure S11E and Figure S12E).

We found six genes in which the phenotype of the RNAi/Smad2^{PM} combination resulted in a synergistic effect ("R*") of strongly reduced wing size (*CG5313-i*; Figure S11T') or an increase in the thickening of the veins compared to the expression of the RNAi alone (Figure S12). Some of the genes that showed thickening of the veins, including O-fucosyltransferase (*CG12366*) and presenilin-enhancer (*CG33198*), belong to the Notch signaling pathway. The synergistic effect of vein thickening suggests that, during pupal development, Smad2^{PM} promotes vein differentiation, and that this effect cannot be compensated for in a situation of reduced Notch signaling.

ChIP with Smad2^{PM}

As a further analysis to identify *bona fide* Smad2 target genes in the wing, we undertook ChIP experiments in wing discs expressing a tagged form of activated Smad2 (*nub-Gal4/UAS-HA-Smad2^{PM}*). In these discs, we could find nuclear and cytoplasmic localization of HA-Smad2^{PM} (Figure S13). We found a large number of statistically significant DNA regions (peaks) bound by HA-Smad2^{PM} even at the lower FDR used (Table S5). These peaks were associated to the closest coding regions located in their genomic proximity including 10 kb, identifying a large collection of candidate target genes: 759 (FDR1), 2277 (FDR5), 3719 (FDR10), or 8954 (FDR25) (Table S5). The presence of peaks associated to genes is indicated for the 200 genes selected in the microarray (Table

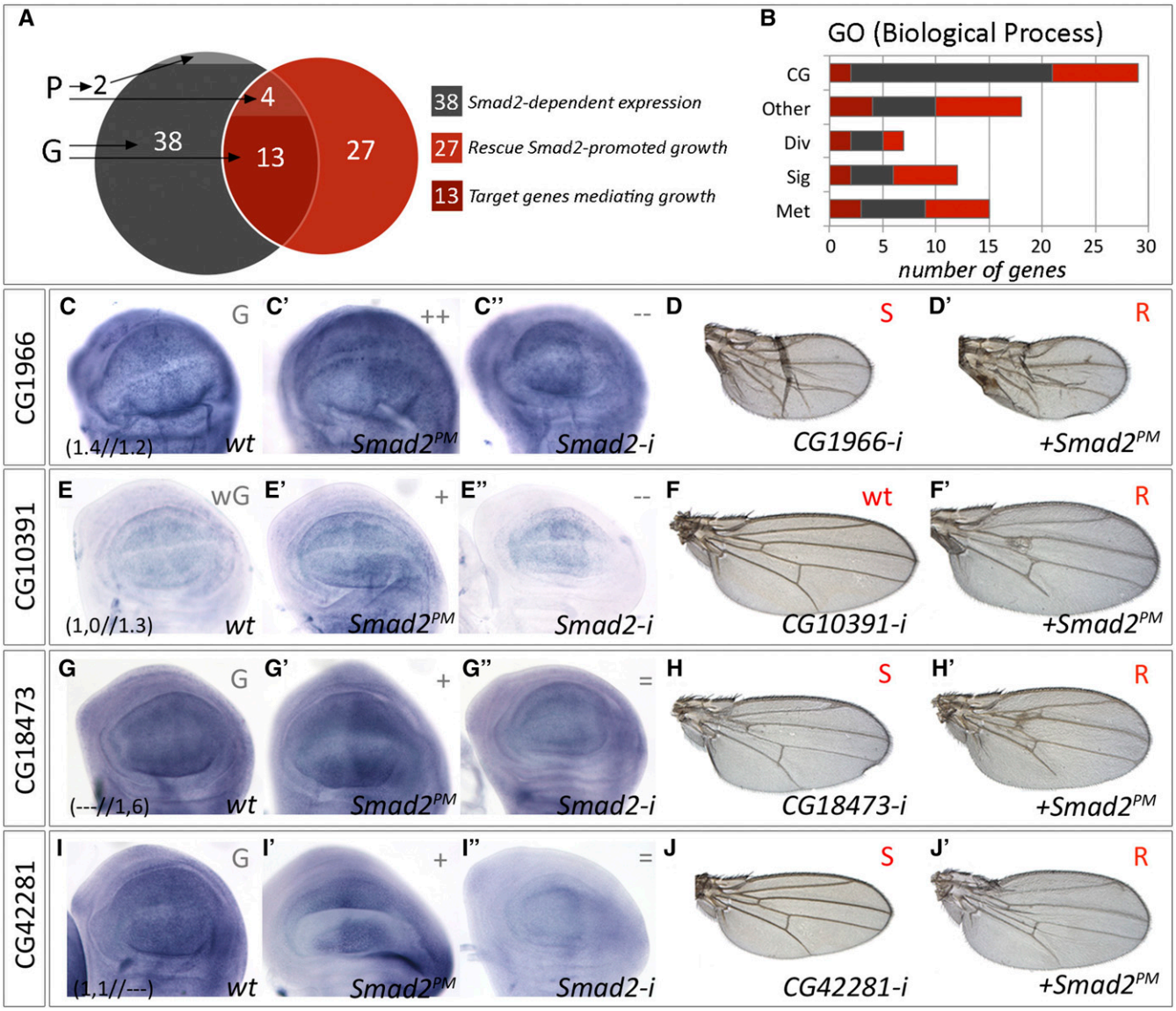

Figure 8 Expression and phenotypic analysis of the best Smad2 downstream candidate genes. (A) Overlap between the group of genes that shows a Smad2-dependent expression pattern (gray) and those genes in which loss-of-function rescues the Smad2^{PM} large wing phenotype (red). G and P indicate genes with generalized or patterned expression, respectively. (B) Representation of the number of genes within the anterior groups related to the gene ontology (GO) categories Metabolism (Met), Cell division (Div), Cell signaling (Sig), and others. Genes with no GO terms annotated are included in the group called CG. (C–J) *CG1966*, *CG10391*, *CG18473*, and *CG42281* are representative examples of candidate Smad2 target genes mediating wing growth identified in our screen. These genes present changes (±) in their generalized pattern of expression (C, E, G, and I) in *Smad2* mutant conditions [overexpression of Smad2^{PM} in (C′, E′, G′, and I′) and reduction in (C′′, E′′, G′′, and I′′)], show a requirement for wing growth (D, F, H, and J) and also rescue the Smad2^{PM} overgrowth phenotype (D′, F′, H′, and J′). WT, wild-type.

S4) and for the genes selected as Smad2 candidate targets (Table 1). Only 16 genes out of 200 microarray genes present a peak at FDR1, but we could not find enriched binding motifs analyzing the sequences associated to these peaks, in agreement with the poor specificity of Smad–DNA binding (Massagué *et al.* 2005).

Selected best candidates

We selected as best candidates all genes with a confirmed change in expression identified by *in situ* hybridization (category 1) and all genes in which loss-of-function was able to rescue the Smad2^{PM}-promoted overgrowth (category 2). We considered that the most relevant candidates to understand how Smad2 promotes wing growth were those genes that meet both criteria and were expressed in a generalized manner (Figure 8A). GO terms associated to genes ubiquitously expressed in the wing disc included different aspects of metabolism (*e.g.*, RedOx balance and carbohydrate metabolism), cell signaling, and cell division (Figure 8B). Of the selected genes, 39% did not have previously described biological functions.

Three points are worth mentioning when considering the set of 67 genes included in categories 1 and 2 (Figure 8A).

First, not all genes required for Smad2 function and for which expression *in situ* changes in response to Smad2 are transcribed in a completely ubiquitous manner. For example, *CG6055* (Figure S3B–B") expression is at its highest levels in the presumptive wing veins and wing margin, respectively, and this expression is strongly dependent on Smad2 activity. Conversely, *CG1342*, which is one of a few cases of genes negatively regulated by the pathway, is mostly expressed in intervein territories (Figure 6, I–I"). An extreme example of a gene regulated by Smad2 and expressed in a highly restricted spatial pattern is exemplified by *CG8084* (*ana*), which is only expressed in four clusters of cells located in proximal anterior and posterior wing territories (Figure S3C). The expression of *ana* in these clusters strongly depends on Smad2 activity, and we mapped the regulatory region mediating this effect to a 2396-bp genomic fragment located in the 5′ region of the gene (*anaRR*) (Figure S14A). Additionally, we found other genomic fragments in the proximity of the *ana* coding region that function as regulatory modules of *ana* expression in the eye disc, brain, salivary glands, and ring gland (Figure S14, B–G). Interestingly, all these tissues are territories of P-Smad2 accumulation (Hevia and de Celis 2013).

The second relevant point is that not all of the genes whose generalized expression is regulated by Smad2 are individually required for Smad2 function in the wing. This set of 38 genes (Figure 8A, not overlapping section of the gray group) might identify canonical targets of Smad2 with minor individual contributions to the *Smad2* phenotype in the wing disc. Finally, we identified a group of 27 genes that might be functionally related to Smad2, because their loss-of-function condition is able to suppress the extra growth induced by $Smad2^{PM}$, but for which we could not detect changes in their *in situ* pattern of expression in response to Smad2 (Figure 8A, not overlapping section of the red group). This set of genes might correspond to targets of Smad2 with a significant functional relevance in implementing Smad2 activity, but for which this protein has a weak impact on their transcriptional regulation.

After these analyses, we singled out a group of 17 genes, 13 of which expressed in all cells of the wing epithelium in a Smad2-dependent manner and whose functions are required for growth regulation downstream of Smad2. These 13 genes include: proteins implicated in cell signaling and transport activity such as the transcription factors *CG42281* (*bun*; Figure 8, I–J') and *CG12399* (*mad*), the subunit of a chromatin assembly complex *CG1966* (Acf1; Figure 8, C–D'), the ionic channel *CG1058* (*rpk*), the kinase *CG11221* (*Pkn*), the *Laminin IV CG42677* (*wb*), the vacuolar ATPase *CG6737* (*Vha16-5*), and the phosphatase *CG10089*, as well as proteins containing enzymatic motifs potentially related to cellular metabolism such as the cytochrome P450 component *CG10391* (*Cyp310a1*; Figure 8, E–F'), the phosphotriesterase-related protein *CG18473* (Figure 8, G–H'), the glucose-6-phosphate 1-epimerase *CG9008* (see Figure 6, H–H"), and unknown genes such as *CG6434* (Figure S6, AB and AB") and *CG8420* (Figure S5, M–M").

One Smad2 target candidate is *CG9008*, the gene encoding the glycolytic enzyme glucose-6-phosphate 1-epimerase. The expression of *CG9008* responds to changes in Smad2 (Figure 6, H and H'), and its knockdown reduces wing size and suppresses the overgrowth caused by $Smad2^{PM}$ expression (Figure 9, A and B). Glycolysis is a sequence of 10 enzymatic reactions that transform glucose into ATP, NADH, and two molecules of pyruvate,. We explored the possibility of a requirement for other glycolytic enzymes in the acquisition of a normal wing size and found that, in addition to *CG9008*, the knockdown of *CG6058* (aldolase; Figure 9D), *CG7070* (pyruvate kinase; not shown), and *CG8893* (glyceraldehyde 3-phosphate dehydrogenase; Figure 9G) causes a reduced wing size phenotype. Furthermore, knockdown of *CG9008* (Figure 9, B and F), *CG8893* (Figure 9, H and F), and *CG6058* (Figure 9, E and F) rescues the $Smad2^{PM}$ phenotype, suggesting that Smad2 might influence the efficiency of glycolysis and therefore contribute to the metabolic fitness of imaginal cells. We also tested the knockdown of other glycolytic enzymes including *CG3001* (*HexA*), *CG32849* (*Hex-t2*), *CG8094* (*Hex-C*), *CG33102* (*Hex-t1*), *CG4001* (*Pfk*), *CG2171* (*Tpi*), *CG3127* (*Pgk*), *CG14816* (*Pgam5*), *CG15874* (*Pgam5-2*), and *CG17654* (*Eno*). In all cases, the expression of these RNAi in the wing (*UAS-dicer2/+*; *nub-Gal4/UAS-RNAi*) did not affect its size, perhaps because of functional redundancy. Knockdown of these genes does not modify the overgrowth phenotype caused by expression of $Smad2^{PM}$ (see for example Figure 9, J and K).

Discussion

The *Drosophila* wing disc is a convenient experimental system to identify and analyze genes controlling or affecting growth in an epithelial tissue. The proliferation of imaginal cells is regulated by a variety of signaling pathways and transcriptional regulators, but we still have a limited knowledge of the molecular mechanisms underlying the ordered progression through the cell cycle and its coupling with cellular growth. Some of the components affecting cell proliferation, such as proteins regulating cell cycle transitions, display an absolute functional requirement and, in their absence, cell division is halted (Edgar *et al.* 1994; Duronio *et al.* 1998). In stark contrast, mutations affecting the biosynthetic capacity of the cell only affect cell division rates. This is one key aspect of Smad2 contribution to imaginal growth, because its function is only necessary to sustain the appropriate division rates needed for the imaginal discs to reach their normal size. A similar requirement for Smad2 is observed in *Drosophila* neuroblasts, where TGFβ signaling enhances cell proliferation but is not absolutely required for cell division (Zhu *et al.* 2008). In other cellular contexts, such as vertebrate epithelial, neural, and hematopoietic cells, TGFβ signaling exerts negative regulation on cell cycle progression (Massagué and Wotton 2000), indicating that the relationship between the pathway and cell proliferation depends on the cellular context (Massagué and Wotton 2000). Because it is the

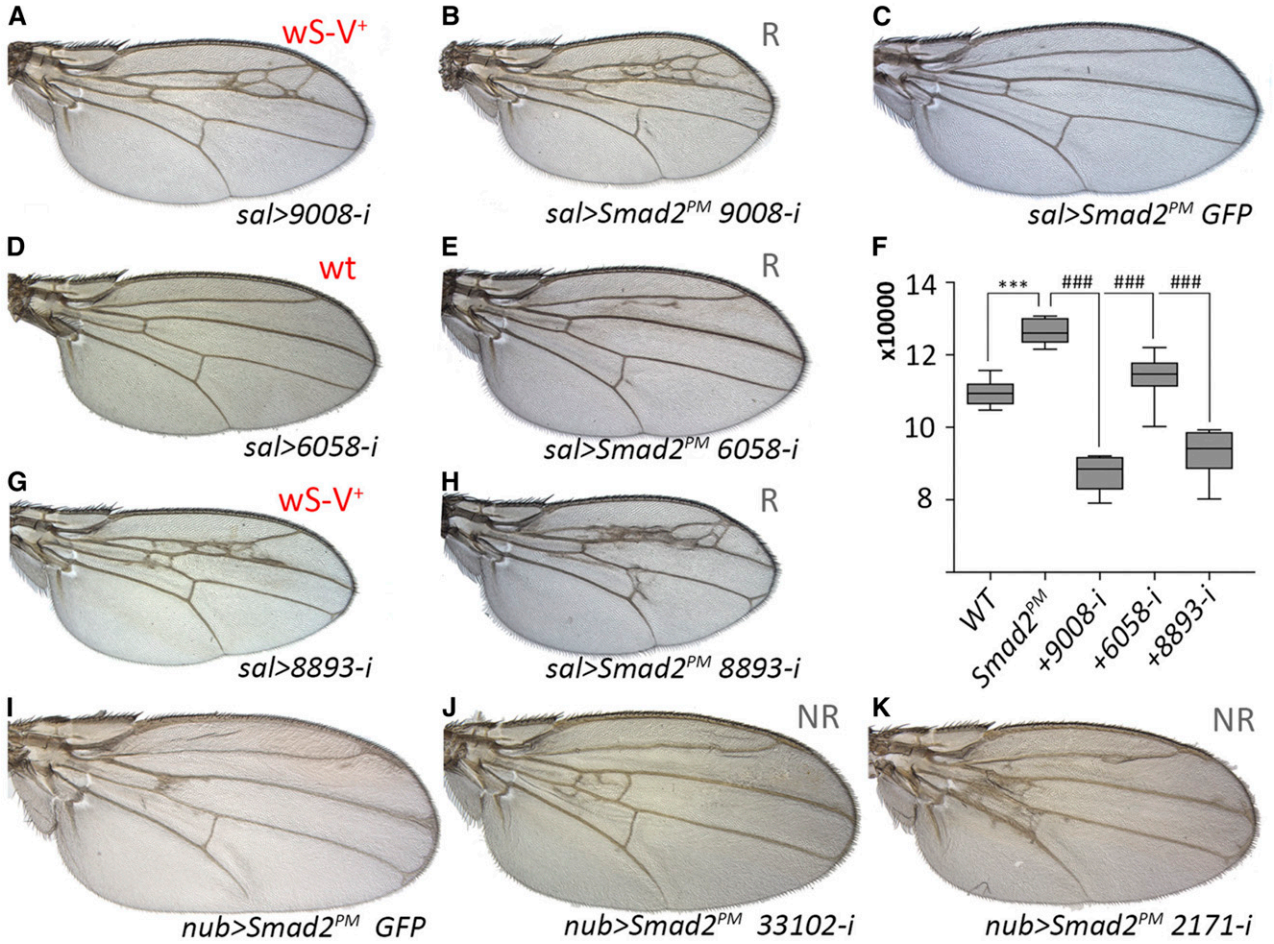

Figure 9 Effects on wing size caused by knockdown of genes encoding glycolytic enzymes. (A) *UAS-dicer2*/+; *sal^{EPv}-Gal4*/+; *UAS-CG9008i*/+. (B) *UAS-dicer2*/+; *sal^{EPv}-Gal4*/+; *UAS-Smad2^{PM}*/*UAS-CG9008i*. (C) *UAS-dicer2*/+; *sal^{EPv}-Gal4*/*UAS-GFP*; *UAS-Smad2^{PM}*/+. (D) *UAS-dicer2*/+; *sal^{EPv}-Gal4*/+; *UAS-CG6058i*/+. (E) *UAS-dicer2*/+; *sal^{EPv}-Gal4*/+; *UAS-Smad2^{PM}*/*UAS-CG6058i*. (F) Wing size measurements of *UAS-dicer2*/+; *sal^{EPv}-Gal4*/+; *UAS-Smad2^{PM}*/+ in combination with *UAS-GFP* (control), *UAS-CG9008i* (+9008-i), *UAS-CG6058i* (+6058-i) and *UAS-CG8893i* (+8893-i). (G) *UAS-dicer2*/+; *sal^{EPv}-Gal4*/+; *UAS-CG8893i*/+. (H) *UAS-dicer2*/+; *sal^{EPv}-Gal4*/+; *UAS-Smad2^{PM}*/*UAS-CG8893i*. The combination between Smad2^{PM} and 9008-i, 6058-I, or 8893-i, in all the cases rescue (R) the overgrowth caused by Smad2^{PM} alone. (I–K) Example of combinations in which knockdown does not rescue (NR) the Smad2^{PM} phenotype: *UAS-dicer2*/+; *nub-Gal4 UAS-GFP*/*UAS-Smad2^{PM}* (control), *UAS-dicer2*/+; *nub-Gal4 UAS- Smad2^{PM}*/*UAS-CG33102i* (J) and *UAS-dicer2*/+; *nub-Gal4 UAS- Smad2^{PM}*/*UAS-CG2171i* (K). WT, wild-type.

repertoire of cofactors and available target genes of the pathway in each cellular setting that defines the cellular response to signaling, a necessary step to understand the function of Smad2 in promoting cell division in imaginal cells is the identification of Smad2-interacting proteins and its target downstream genes.

In this work, we have analyzed the contribution of Smad2 to wing growth, aiming to identify candidate downstream genes of the Smad2 transcriptional regulator with a role in the control of wing size. We have taken multiple approaches to identify Smad2 target genes, including the analysis of its interaction with different signaling pathways and unbiased approaches. In the first case, we focused on the HSW and InR signaling pathways (Britton *et al.* 2002; Oh and Irvine 2010) and found that Smad2 cooperates with both pathways to promote cell proliferation. However, it appears that the three pathways function as independent inputs regulating different sets of target genes. In agreement, we could not find any evidence of direct cooperation between Smad2 and Yki to regulate the transcription of Yki target genes. We identified an input from Smad2 into the regulation of *stg* and *CycE*, as the expression of activated Smad2 is able to promote their transcription. In this manner, Smad2 could be a participant in the complex regulatory machinery of *stg* and *CycE* transcription, although its function is not absolutely required for the expression of these genes. Conversely, Smad2 must operate through additional targets to influence cell proliferation, since *stg* or *CycE* overexpression cannot rescue the Smad2 mutant phenotype.

As a complementary approach to identify the mechanisms underlying the effect of Smad2 on imaginal cell proliferation, we undertook microarray and ChIP experiments. In the first case, we compared the expression profiles of wild-type cells with those of *Smad2* loss- and gain-of-function conditions. In

the second case, we identified DNA regions bound by a tagged Smad2 protein that was overexpressed in all wing cells. The result of expression arrays uncovered a multitude of changes in the wing transcriptional landscape in *Smad2* mutant conditions. Many of the changes that we identified were of small magnitude, and we were able to confirm changes by *in situ* hybridization experiments in only 29% of the cases analyzed. This result suggests that Smad2 might have a weak to moderate impact on the modulation of expression of a large collection of target genes. This scenario is compatible with the ChIP data that we obtained in conditions of overexpression of HA-Smad2^{PM}, because the binding of this protein to the DNA was widespread and associated with a large number of sites and associated genes. The analysis of the sequences bound by Smad2 did not uncover enriched DNA motifs, which is expected considering the limited resolution of ChIP–chip data and the fact that binding might be determined by other cofactor proteins participating in transcriptional complexes, including Smad2/Smad4 oligomers (Massagué and Wotton 2000; Massagué *et al.* 2005). As a note of caution, the ChIP experiments were undertaken in wing discs with Smad2^{PM} overexpression, a situation that might be prone to detect weak Smad2–DNA interactions and therefore mask the existence of enriched binding sites.

The microarray experiments uncovered candidate Smad2 target genes and, out of 200 that we were able to analyze by *in situ* hybridization, we detected strong changes in the expression pattern of 57 genes in response to Smad2 modifications. Interestingly, the overwhelming majority of these genes were expressed in a generalized pattern in imaginal discs, in coincidence with the spatial domain of phospho-Smad2 accumulation. Furthermore, most of these genes behaved as targets activated by the pathway, because their expressions were reduced in *Smad2* loss-of-function conditions or increased in response to Smad2^{PM}. The identification of this collection of genes contributes to the understanding of the events downstream of TGFβ signaling. To complement the expression analysis, we undertook a preliminary functional characterization of the genes selected by microarrays. Because Smad2 positively regulates the expression of most of them, our approach consisted of looking for functional requirements in loss-of-function conditions generated by the expression of RNAi. For the majority of genes (63%), we did not find a loss-of-function phenotype in the wing, suggesting that their contribution is minor, redundant, or that RNAi expression was not enough to reveal a functional requirement.

We also identified a group of genes that, when downregulated by RNAi expression, resulted in a mutant phenotype consisting of reductions in wing size with or without effects on vein patterning. Certainly, these genes are the most likely candidates to mediate the growth-promoting function of Smad2. Most genes affecting wing size are required for Smad2^{PM} to promote extra wing growth. This epistatic relationship could be indicative of a functional requirement downstream of Smad2, but it is also compatible with functions independent of Smad2. However, the changes in gene expression observed in *Smad2* mutant backgrounds suggest that they might act as downstream mediators of Smad2 function. Our best candidate genes include a multiplicity of molecular functions, suggesting that Smad2 activity involves a widespread modulation of a variety of cellular processes rather than a single functional input. Within the group of 13 genes selected as best candidate Smad2 targets, some examples are of particular interest because they have been previously associated with cell proliferation and cellular metabolism, or linked to TGFβ signaling in other cellular settings. For example, *CG42281* (*bun*) encodes a leucine zipper transcription factor necessary for cell proliferation during *Drosophila* development, and its function is necessary to promote division in wing imaginal cells (Gluderer *et al.* 2008; Wu and Chiang 2008). Interestingly, the *bun* human ortholog is TSC-22 (transforming growth factor-β1 stimulated clone-22), a candidate tumor suppressor gene (Kim *et al.* 2009), originally identified as a transcriptionally activated TGF-β1 target gene (Shibanuma *et al.* 1992). Another candidate is *CG10391* (*Cyp310a1*), which belongs to the cytochrome P450 family, a large group of 86 proteins with oxidoreductase activity that participate in catalytic processes important during development and detoxification of foreign compounds. Remarkably, *Cyp310a1* is the only member of this family that is expressed in the wing disc (Chung *et al.* 2009). Another example is *CG1966* (Acf1), which is the fly ortholog of human BAZ1A (Ito *et al.* 1997; Chioda *et al.* 2010), a component of the conserved ISWI chromatin remodeler controlling chromatin assembly and nucleosome remodelling (Erdel *et al.* 2011; Bartholomew 2014). ISWI function has been linked to cell cycle progression and metabolism in genetic screens (Arancio *et al.* 2010), suggesting that the modulation of its expression level is important to sustain imaginal disc proliferation. Other examples of Smad2 candidate target genes include *CG18473*, encoding a phosphotriesterase-related protein, the human ortholog of which (PTER) is involved in albumin sensing (Cheng *et al.* 2014), and *CG9008*, a glucose-6-phosphate 1-epimerase that could be involved in carbohydrate metabolism. Remarkably, other enzymes involved in glycolysis such as *CG7070* (pyruvate kinase), *CG8893* (glyceraldehyde 3-phosphate dehydrogenase 2), or *CG6058* (aldolase) are similarly required to *CG9008* during wing development, and knockdown of *CG6058* and *CG8893* also reduces the extra wing growth stimulated by Smas2^{PM}.

The relationship between Smad2 and cellular metabolism certainly requires further investigation, but the available evidence suggests that Smad2 could modulate the metabolic fitness of epidermal cells and that alteration of fitness in *Smad2* mutant conditions results in changes in cell proliferation rhythms. This proposal is compatible with recent findings linking TGFβ activity to the regulation of cellular and mitochondrial metabolism in *Drosophila* larvae (Ghosh and O'Connor 2014), and with the regulation in the midgut of digestive enzymes that participate in sugar metabolism (Chung *et al.* 2009).

Acknowledgments

We are grateful to the Developmental Studies Hybridoma Bank at the University of Iowa, the National Institute of Genetics (Japan) Fly Stocks, the Bloomington *Drosophila* Stock Center, and the Vienna *Drosophila* RNAi Center for providing the tools necessary for this work. We also thank M. F. Organista, M. Martín, N. Barrios, and A. Baonza for sharing some probes for *in situ* hybridization assays. C. Estella, A. Baonza, and C. Martínez-Ostalé are acknowledged for criticism that improved the manuscript, and S. Russell and B. Fischer (University of Cambridge and Cambridge Systems Biology Centre) for help with chromatin immunoprecipitation (ChIP)-on-chip assays and data processing. This work was funded by grant BFU2015-64220-P from Mineco. Institutional support to the Centro de Biología Molecular Severo Ochoa from the Banco de Santander, and Fundación Ramón Areces is also acknowledged. The funding bodies did not participate in the design of the study, collection, analysis, and interpretation of data, or in writing the manuscript. The authors declare that they have no competing interests.

Author contributions: C.F.H. and J.F.d.C. designed the work and analyzed the data. A.L.-V. and N.E. participated in the collection of samples and elaboration of microscopic preparations. J.F.d.C. wrote the manuscript with the support of C.F.H.

Literature Cited

Arancio, W., M. C. Onorati, G. Burgio, M. Collesano, A. M. Ingrassia *et al.*, 2010 The nucleosome remodeling factor ISWI functionally interacts with an evolutionarily conserved network of cellular factors. Genetics 185: 129–140.

Bartholomew, B., 2014 Regulating the chromatin landscape: structural and mechanistic perspectives. Annu. Rev. Biochem. 83: 671–696.

Boedigheimer, M., P. Bryant, and A. Laughon, 1993 Expanded, a negative regulator of cell proliferation in Drosophila, shows homology to the NF2 tumor suppressor. Mech. Dev. 44: 83–84.

Britton, J. S., W. K. Lockwood, L. Li, S. M. Cohen, and B. A. Edgar, 2002 Drosophila's insulin/PI3-kinase pathway coordinates cellular metabolism with nutritional conditions. Dev. Cell 2: 239–249.

Brummel, T., S. Abdollah, T. E. Herry, M. J. Shimell, J. Merrian *et al.*, 1999 The *Drosophila* activin receptor baboon signals through dSmad2 and controls cell proliferation but not patterning during larval development. Genes Dev. 13: 98–111.

Bryant, P. J., and P. Simpson, 1984 Intrinsic and extrinsic control of growth in developing organs. Q. Rev. Biol. 59: 387–415.

Calleja, M., E. Moreno, S. Pelaz, and G. Morata, 1996 Visualization of gene expression in living adult *Drosophila*. Science 274: 252–255.

Chen, C. L., M. C. Schroeder, M. Kango-Singh, C. Tao, and G. Halder, 2012 Tumor suppression by cell competition through regulation of the hippo pathway. Proc. Natl. Acad. Sci. USA 109: 484–489.

Cheng, C.-W., L.-C. Chang, T.-L. Tseng, C.-C. Wu, Y.-F. Lin *et al.*, 2014 Phosphotriesterase-related protein sensed albuminuria and conferred renal tubular cell activation in membranous nephropathy. J. Biomed. Sci. 21: 32.

Chioda, M., S. Vengadasalam, E. Kremmer, A. Eberharter, and P. B. Becker, 2010 Developmental role for ACF1-containing nucleosome remodellers in chromatin organisation. Development 137: 3513–3522.

Chung, H., T. Sztal, S. Pasricha, M. Sridhar, P. Batterham *et al.*, 2009 Characterization of Drosophila melanogaster cytochrome P450 genes. Proc. Natl. Acad. Sci. USA 106: 5731–5736.

Cruz, C., A. Glavic, M. Casado, and J. F. de Celis, 2009 A gain-of-function screen identifying genes required for growth and pattern formation of the Drosophila melanogaster wing. Genetics 183: 1005–1026.

de Celis, J. F., 1997 Expression and function of decapentaplegic and thick veins during the differentiation of the veins in the Drosophila wing. Development 124: 1007–1018.

Derynck, R., R. J. Akhurst, and A. Balmain, 2001 TGF-beta signaling in tumor suppression and cancer progression. Nat. Genet. 29: 117–129 (erratum: Nat. Genet. 29: 351).

Duronio, R. J., P. C. Bonnette, and P. H. O'Farrell, 1998 Mutations of the Drosophila dDP, dE2F, and cyclin E genes reveal distinct roles for the E2F-DP transcription factor and cyclin E during the G1-S transition. Mol. Cell. Biol. 18: 141–151.

Edgar, B. A., 2006 How flies get their size: genetics meets physiology. Nat. Rev. Genet. 7: 907–916.

Edgar, B. A., D. A. Lehman, and P. H. O'Farrell, 1994 Transcriptional regulation of *string* (*cdc25*): a link between developmental programming and the cell cycle. Development 120: 3131–3143.

Edgar, B. A., J. Britton, A. F. de la Cruz, L. A. Johnston, D. Lehman *et al.*, 2001 Pattern- and growth-linked cell cycles in Drosophila development. Novartis Found. Symp. 237**:** 3–12; discussion 12–18, 36–42.

Erdel, F., J. Krug, G. Langst, and K. Rippe, 2011 Targeting chromatin remodelers: signals and search mechanisms. Biochim. Biophys. Acta 1809: 497–508.

Feng, X. H., and R. Derynck, 2005 Specificity and versatility in tgf-beta signaling through Smads. Annu. Rev. Cell Dev. Biol. 21: 659–693.

Gesualdi, S. C., and T. E. Haerry, 2007 Distinct signaling of Drosophila activin/TGF-beta family members. Fly (Austin) 1: 212–221.

Ghosh, A. C., and M. B. O'Connor, 2014 Systemic activin signaling independently regulates sugar homeostasis, cellular metabolism, and pH balance in Drosophila melanogaster. Proc. Natl. Acad. Sci. USA 111: 5729–5734.

Gibbens, Y. Y., J. T. Warren, L. I. Gilbert, and M. B. O'Connor, 2011 Neuroendocrine regulation of Drosophila metamorphosis requires TGFbeta/activin signaling. Development 138: 2693–2703.

Gluderer, S., S. Oldham, F. Rintelen, A. Sulzer, C. Schutt *et al.*, 2008 Bunched, the Drosophila homolog of the mammalian tumor suppressor TSC-22, promotes cellular growth. BMC Dev. Biol. 8: 10.

Herboso, L., M. M. Oliveira, A. Talamillo, C. Perez, M. Gonzalez *et al.*, 2015 Ecdysone promotes growth of imaginal discs through the regulation of Thor in D. melanogaster. Sci. Rep. 5: 12383.

Hevia, C. F., and J. F. de Celis, 2013 Activation and function of TGFbeta signalling during Drosophila wing development and its interactions with the BMP pathway. Dev. Biol. 377: 138–153.

Huang da, W., B. T. Sherman, and R. A. Lempicki, 2009 Systematic and integrative analysis of large gene lists using DAVID bioinformatics resources. Nat. Protoc. 4: 44–57.

Ito, T., M. Bulger, M. J. Pazin, R. Kobayashi, and J. T. Kadonaga, 1997 ACF, an ISWI-containing and ATP-utilizing chromatin assembly and remodeling factor. Cell 90: 145–155.

Johnston, L. A., and P. Gallant, 2002 Control of growth and organ size in Drosophila. Bioessays 24: 54–64.

Kim, J., S. Lee, M. Hwang, S. Ko, C. Min *et al.*, 2009 Bunched specifically regulates alpha/beta mushroom body neuronal cell proliferation during metamorphosis. Neuroscience 161: 46–52.
Leevers, S. J., B. Vanhaesebroeck, and M. D. Waterfield, 1999 Signalling through phosphoinositide 3-kinases: the lipids take centre stage. Curr. Opin. Cell Biol. 11: 219–225.
Massagué, J., 2012 TGF-beta signaling in development and disease. FEBS Lett. 586: 1833.
Massagué, J., and D. Wotton, 2000 Transcriptional control by the TGF-beta/Smad signaling system. EMBO J. 19: 1745–1754.
Massagué, J., J. Seoane, and D. Wotton, 2005 Smad transcription factors. Genes Dev. 19: 2783–2810.
Milan, M., S. Campuzano, and A. Garcia-Bellido, 1996 Cell cycling and patterned cell proliferation in the wing primordium of *Drosophila*. Proc. Natl. Acad. Sci. USA 93: 640–645.
Molnar, C., M. Resnik-Docampo, M. Organista, M. Martin, C. F. Hevia et al., 2011 Signalling pathways in development and human disease: a Drosophila wing perspective, pp. 1–37 in *Human Genetic Diseases*, edited by D. E. Plaseska-Karanfilska. InTech Publisher, New York.
Neto-Silva, R. M., B. S. Wells, and L. A. Johnston, 2009 Mechanisms of growth and homeostasis in the Drosophila wing. Annu. Rev. Cell Dev. Biol. 25: 197–220.
Nicol, J. W., G. A. Helt, S. G. Blanchard, Jr., A. Raja, and A. E. Loraine, 2009 The integrated genome browser: free software for distribution and exploration of genome-scale datasets. Bioinformatics 25: 2730–2731.
Oh, H., and K. D. Irvine, 2010 Yorkie: the final destination of Hippo signaling. Trends Cell Biol. 20: 410–417.
Oh, H., and K. D. Irvine, 2011 Cooperative regulation of growth by Yorkie and Mad through bantam. Dev. Cell 20: 109–122.
Orme, M. H., S. Alrubaie, G. L. Bradley, C. D. Walker, and S. J. Leevers, 2006 Input from Ras is required for maximal PI(3)K signalling in Drosophila. Nat. Cell Biol. 8: 1298–1302.
Peterson, A. J., P. A. Jensen, M. Shimell, R. Stefancsik, R. Wijayatonge *et al.*, 2012 R-Smad competition controls activin receptor output in Drosophila. PLoS One 7: e36548.
Prober, D. A., and B. A. Edgar, 2002 Interactions between Ras1, dMyc, and dPI3K signaling in the developing Drosophila wing. Genes Dev. 16: 2286–2299.
Ryoo, H. D., A. Bergmann, H. Gonen, A. Ciechanover, and H. Steller, 2002 Regulation of Drosophila IAP1 degradation and apoptosis by reaper and ubcD1. Nat. Cell Biol. 4: 432–438.
Sander, V., E. Eivers, R. H. Choi, and E. M. De Robertis, 2010 Drosophila Smad2 opposes Mad signalling during wing vein development. PLoS One 5(4): e10383.
Sandmann, T., J. S. Jakobsen, and E. E. Furlong, 2006 ChIP-on-chip protocol for genome-wide analysis of transcription factor binding in Drosophila melanogaster embryos. Nat. Protoc. 1: 2839–2855.
Shi, Y., and J. Massagué, 2003 Mechanisms of TGF-beta signaling from cell membrane to the nucleus. Cell 113: 685–700.
Shibanuma, M., T. Kuroki, and K. Nose, 1992 Isolation of a gene encoding a putative leucine zipper structure that is induced by transforming growth factor β1 and other growth factors. J. Biol. Chem. 267: 10219–10224.
Thacker, S. A., P. C. Bonnette, and R. J. Duronio, 2003 The contribution of E2F-regulated transcription to Drosophila PCNA gene function. Curr. Biol. 13: 53–58.
Toedling, J., O. Skylar, T. Krueger, J. J. Fischer, S. Sperling *et al.*, 2007 Ringo–an R/Bioconductor package for analyzing ChIP-chip readouts. BMC Bioinformatics 8: 221.
Varelas, X., R. Sakuma, P. Samavarchi-Tehrani, R. Peerani, B. M. Rao *et al.*, 2008 TAZ controls Smad nucleocytoplasmic shuttling and regulates human embryonic stem-cell self-renewal. Nat. Cell Biol. 10: 837–848.
Wu, C. L., and A. S. Chiang, 2008 Genes and circuits for olfactory-associated long-term memory in Drosophila. J. Neurogenet. 22: 257–284.
Zhu, C. C., J. Q. Boone, P. A. Jensen, S. Hanna, L. Podemski *et al.*, 2008 Drosophila activin- and the activin-like product Dawdle function redundantly to regulate proliferation in the larval brain. Development 135: 513–521.

Communicating editor: I. K. Hariharan